Key Points:
- Exhumed rocks from subduction zones are on average warmer than models predictions for global subduction zones
- Arbitrary warming below the forearc makes the models conform with the rock record but conflicts with independent observations
- The discrepancy between the rock record and models is explained by preferential exhumation of oceanic crust under warm conditions

Supporting Information:
- Supporting Information S1
- Data Set S1

Correspondence to:
P. E. van Keken,
pvankeken@carnegiescience.edu

Mafic High-Pressure Rocks Are Preferentially Exhumed From Warm Subduction Settings

Peter E. van Keken[1] (ID), **Ikuko Wada[2]** (ID), **Geoffrey A. Abers[3]**, **Bradley R. Hacker[4]** (ID), and **Kelin Wang[5,6]** (ID)

[1]Department of Terrestrial Magnetism, Carnegie Institution for Science, Washington, DC, USA, [2]Department of Earth Sciences, University of Minnesota, Twin Cities, Minneapolis, MN, USA, [3]Department of Earth and Atmospheric Sciences, Cornell University, Ithaca, NY, USA, [4]Department of Earth Science, University of California, Santa Barbara, CA, USA, [5]Pacific Geoscience Centre, Geological Survey of Canada, Natural Resources Canada, Sidney, British Columbia, Canada, [6]School of Earth and Ocean Sciences, University of Victoria, British Columbia, Victoria, Canada

Abstract The oceanic crust that enters a subduction zone is generally recycled to great depth. In rare and punctuated episodes, however, blueschists and eclogites derived from subducted oceanic crust are exhumed. Compilations of the maximum pressure-temperature conditions in exhumed rocks indicate significantly warmer conditions than those predicted by thermal models. This could be due to preferential exhumation of rocks from hotter conditions that promote greater fluid productivity, mobility, and buoyancy. Alternatively, the models might underestimate the forearc temperatures by neglecting certain heat sources. We compare two sets of global subduction zone thermal models to the rock record. We find that the addition of reasonable amounts of shear heating leads to less than 50 °C heating of the oceanic crust compared to models that exclude this heat source. Models for young oceanic lithosphere tend to agree well with the rock record. We test the hypothesis that certain heat sources may be missing in the models by constructing a global set of models that have high arbitrary heat sources in the forearc. Models that satisfy the rock record in this manner, however, fail to satisfy independent geophysical and geochemical observations. These combined tests show that the average exhumed mafic rock record is systematically warmer than the average thermal structure of mature modern subduction zones. We infer that typical blueschists and eclogites were exhumed preferentially under relatively warm conditions that occurred due to the subduction of young oceanic lithosphere or during the warmer initial stages of subduction.

1. Introduction

1.1. Model Predictions for the Thermal Structure of the Forearc in Subduction Zones

In subduction zones, cool oceanic lithosphere enters Earth's mantle and is warmed by its surroundings. The shallow part of the interface between the downgoing oceanic lithosphere and the overriding continental or oceanic plate commonly hosts a seismogenic zone that—over geological time—decouples the motion of the slab from the overriding plate down to a typical depth of 30–40 km (Tichelaar & Ruff, 1993). Below that, the slab appears to remain decoupled from the overriding mantle in an aseismic manner down to a depth of ~75 to 80 km, where the slab starts to couple to the overriding mantle. The resulting corner flow draws hot mantle in from below the arc and backarc, rapidly warming the downgoing oceanic crust (OC) and mantle. The precise mechanics of the change in the coupling is still not fully understood (Wada & Wang, 2009). Metamorphic dehydration reactions in the subducting crust and mantle produce fluids that can travel into the mantle wedge. By lowering the solidus of the mantle the fluids trigger partial melting, leading to arc volcanism (e.g., Gaetani et al., 1993; Grove et al., 2006). Thermal models of subduction zones that include this aseismic extension of the seismogenic zone suggest that the forearc mantle is cold and separated from the hot arc and back-arc mantle by a sharp transition (Syracuse et al., 2010; van Keken et al., 2002; Wada & Wang, 2009). This transition explains various geophysical observations including the rapid change in the forearc surface heat flow and the sharp change in attenuation observed in the forearc and subarc mantle wedge (e.g., Abers et al., 2006; Sacks, 1975; Saita et al., 2015).

Figure 1 shows published case studies for the Washington Cascadia (warm end-member) and Tohoku (cold end-member) margins to demonstrate the sharp change in thermal character between forearc and arc.

It also compares the predicted pressure-temperature (PT) paths in the top of the OC for these two case studies to the global set of models from van Keken et al. (2011). The rapid increase in temperature at the top of the slab at ~2.7 GPa in Figure 1d is due to the coupling between the slab and the hot overriding mantle wedge. The median of the global predictions is skewed to low temperatures due to the global predominance of subduction zones with old incoming plates.

The cold nature of the forearc mantle in subduction zones is a natural consequence of the advection of the low-temperature slab beneath it, which promotes conductive cooling of the forearc. The forearc mantle thermal structure therefore develops somewhat slowly after subduction initiation. If we assume a continental Moho at 40 km depth, a slab coupling point at 80 km depth, and a slab dipping at 45°, the average forearc mantle wedge thickness is $L = 20$ km, from which we can estimate that the forearc establishes itself within the typical conductive time scale of $T_c = L^2/\kappa$, which is 12 Myr with a typical mantle thermal diffusivity $\kappa = 10^{-6}$ m^2/s. This time scale is longer if we take into account cooling of the forearc crust or more steeply dipping slabs. The conductive cooling of the forearc will reach a steady state on such a time scale, indicating that the subducting slab takes significant time to reach thermal equilibrium as well. The long-term thermal structure predicted by thermal models in, for example, Wada and Wang (2009) and Syracuse et al. (2010), applies only to *mature* subduction zones that are sufficiently past their initiation.

The predicted thermal structures tend to agree favorably with various independent geophysical and geochemical observations, such as heat flow (e.g., Hyndman & Peacock, 2003), seismological observations (Abers et al., 2017; Bostock et al., 2002), and studies of arc petrology (e.g., Cooper et al., 2012). In general, temperatures in the forearc need to be cold enough to allow brittle, stick-slip behavior along the megathrust ($\leq$450 °C; Scholz, 1998), while the mantle beneath the arc needs to be hot enough to generate mafic magmas with mantle equilibration temperatures of 1100–1400 °C (Lee et al., 2009).

1.2. Maximum PT Conditions of Exhumed Subduction Zone Mafic Rocks

The good agreement between models and observations does not necessarily extend to the geological record of exhumed subduction zone rocks. Samples derived from subducted OC have been exhumed in the form of eclogites and blueschists from high pressure (HP; 0.5 < P < 2.7 GPa) and ultrahigh pressure (UHP; P > 2.7 GPa; e.g., Agard et al., 2009). The prograde PT paths of these exhumed rocks provide important insights into the conditions of the subducting OC from which they were derived.

We will focus in particular on compilations of maximum PT conditions reported for subduction zone rock (similar to those presented in Agard et al., 2009; Brown & Johnson, 2018; Penniston-Dorland et al., 2015; Tsujimori & Ernst, 2014). A full discussion of regional comparisons is beyond the scope of this paper, but several papers favorably compare rock PT conditions to model predictions (Cook-Kollars et al., 2014; Dragovic et al., 2015; Scambelluri et al., 2016, 2015; Vitale Brovarone & Agard, 2013). Exhumed mafic rocks from >80 km depth are rare (Ernst, 2003), suggesting that eclogitization due to heating at those depths by contact with the hot mantle wedge spells the end of the potential for exhumation of such rocks (Erdman & Lee, 2014; Hacker, 1996; Klemd et al., 2011). A similar rapid increase in temperature at these depths is reported by Stepanov et al. (2016) for subducted and exhumed continental crust.

Notwithstanding the reasonable agreement between these studies and thermal models, the *average* temperature of the subducting slab predicted by the models tends to be up to a few 100 °C lower than the average determined from exhumed subduction zone mafic rocks (Penniston-Dorland et al., 2015; Figure 2). For simplicity we will refer in the remainder of this paper to the petrologically inferred maximum PT conditions of mafic rocks that were exhumed from subduction zones as *the rock record*.

Figure 2 shows a comparison of maximum PT conditions reported in Penniston-Dorland et al. (2015), Agard et al. (2009), and Brown and Johnson (2018). Because the thermal models do not include the process of exhumation or subduction of continental rock, it is appropriate to focus, where possible, on those data points that are for rocks with a clear prograde path and of clear oceanic affinity. Figure 2b shows the resulting prograde-only data set ($N = 77$), which is an update (S. Penniston-Dorland, personal communication, November 2017) to Figure 7 from Penniston-Dorland et al. 2015. We will refer to this prograde-only data set as SPD15p. This frame also shows the low dT/dP data ($N = 105$) from Brown and Johnson 2018 that were identified by these authors to be from oceanic terranes (M. Brown, personal communication, November 2017). The averages of the rock PT (indicated by the solid lines) are similar between the full and prograde-only data sets from Penniston-Dorland et al. (2015) although there are fewer high PT outliers in the latter. The oceanic-only
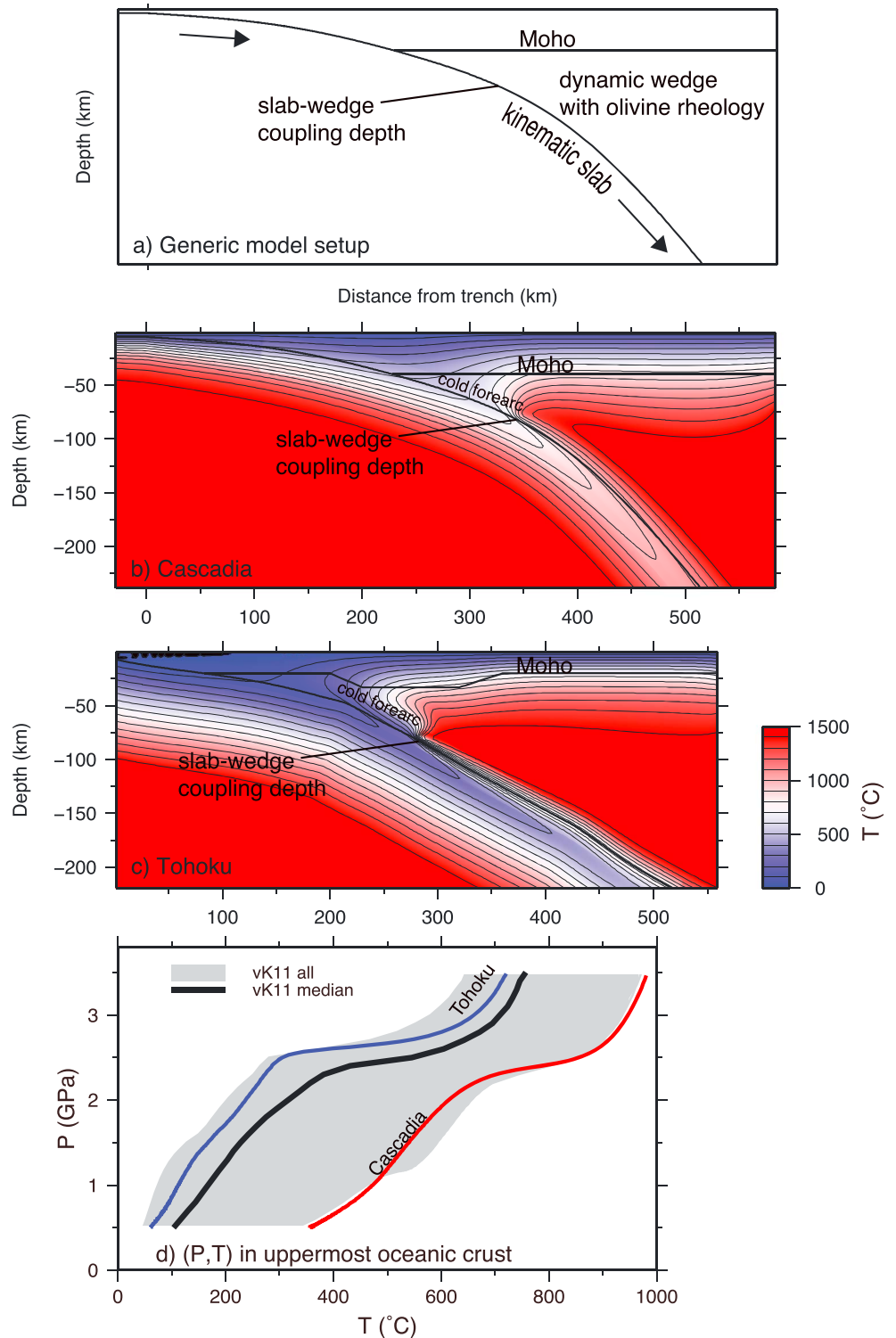
Figure 1. Subduction zone thermal models provide predictions for the thermal state of the oceanic crust from which occasionally blueschists and eclogites are exhumed. (a) Generic model set up of the kinematic-dynamic models considered here; (b) thermal model for Cascadia (the CAFE model from Abers et al., 2013); (c) thermal model for Tohoku (profile T8 from van Keken et al., 2012); (d) Summary of pressure-temperature (PT) conditions in the uppermost oceanic crust from vK11=van Keken et al., (2011; gray field) along with the median of the models in black. The blue and red lines are the conditions in the uppermost oceanic crust from frames b (in red) and c (in blue).
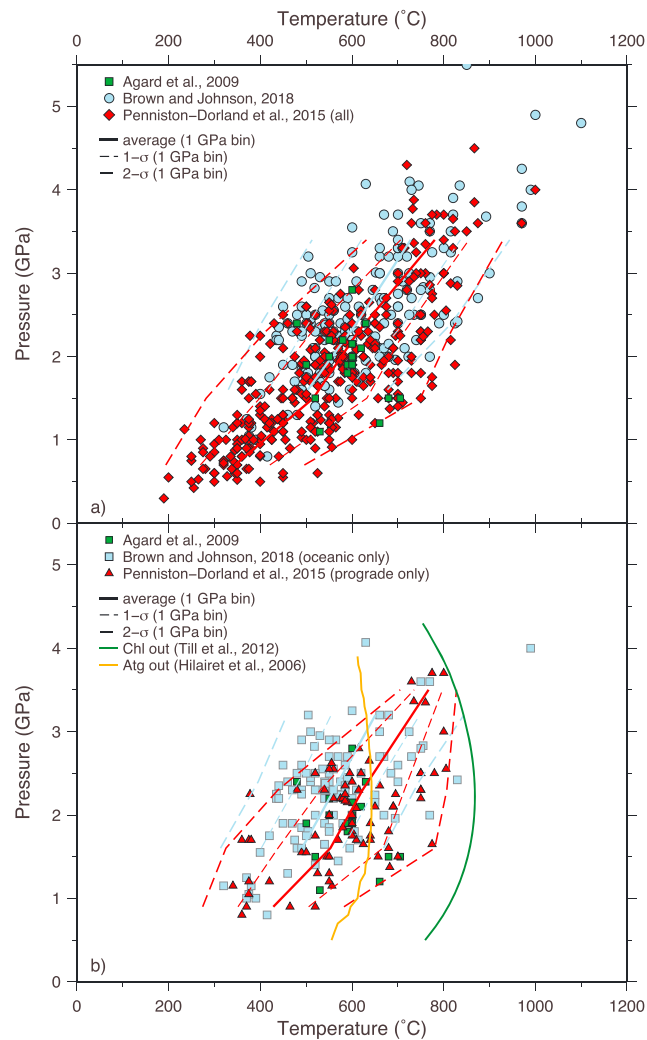
Figure 2. Pressure-temperature compilations of exhumed subduction zone rocks. (a) Comparison of compilation of maximum pressure-temperature conditions recorded in exhumed subduction zone rock from Penniston-Dorland et al., (2015; red diamonds), Brown and Johnson (2018; blue circles), and Agard et al., (2009; green squares). The averages of the Penniston-Dorland et al. (2015) and Brown and Johnson (2018) data sets are indicated in the bold lines of corresponding color. The averages are computed in 1-GPa bins; the one and two standard deviations within those bins are shown in the finely and more coarsely dashed lines, respectively. (b) As in (a) except that showing only those data from Penniston-Dorland et al. (2015) for rocks that have a clear prograde path (red triangles) and only data from Brown and Johnson (2018) that are from oceanic rocks (blue squares). The maximum stability fields of antigorite and chlorite are shown for reference.

data from Brown and Johnson (2018) are about 50 °C cooler on average than their full low dT/dP data set or the SPD15p data. The outer 2σ lines shown for SPD15p in Figure 2b provide a useful outer bound to the rock PT data. For context and later discussion we provide the maximum stability of antigorite (Hilairet et al., 2006) and chlorite (Till et al., 2012) in Figure 2b. We note that the experimentally constrained PT conditions of antigorite stability from Hilairet et al. (2006) agree well with independent recent work (Padrón-Navarta et al., 2010, 2013).

1.3. Relative Volumes of Exhumed Subduction Zone Rocks

The relative amount of OC that is recycled back to Earth's surface is small. From exhumed rocks in the well-studied Western Alps it has been suggested that a maximum of only a few percent of the consumed Liguro-Piemontese OC may be preserved (Agard et al., 2009). For other regions, the volume of subducted OC that was exhumed is estimated to be less than — or much less than — 1% (Agard et al., 2009, their Table 1b). A similar conclusion of rather limited exhumation of rock during warmer-than-normal conditions was reached by Wallis et al. (2009) for the Sanbagawa belt. Simple mass balance calculations also show that nearly all OC

has to be recycled to the deeper Earth. If we assume a total length of the subduction system of 50,000 km, an average OC thickness of 7 km, and an average convergence velocity of 5 cm/year, then 1.75×10^{10} m^3 of OC enters the trench each year. In the last 200 Myr this amounts to 3.5×10^{18} m^3. If all of this had returned to Earth's surface and been added to the continental crust (with an area of 2×10^{14} m^2), this crust would have increased in thickness by 17 km. If the same had happened over 4 Byr, the continental crust would be nearly 400 km thick. Clearly, the recycling of OC has a vanishingly small role in the building of the continental crust.

Agard et al. (2009) also suggested that, in contrast to the exhumation of metasedimentary rocks, the exhumation of rocks from the subducting igneous OC has been punctuated and rare. In a significant number of cases, exhumation occurred either shortly after the onset of subduction or toward the final stages of subduction. Even in long-lived and large-scale subduction systems, such as the one that formed the Zagros mountains, the exhumation of subducted OC has been spatially and volumetrically limited (Agard et al., 2006). Agard et al. (2009) explained these observations as the result of preferential exhumation of rocks from young (and therefore warm and buoyant) oceanic lithosphere, lithosphere shortly after subduction initiation, or from lithosphere shortly after changes in subduction geometry or convergence parameters, which may include the subduction of continental crust. Similarly, Endo et al. (2012) demonstrated that exhumation of the metamorphic rocks in the Sanbagawa belt occurred in two unusually warm stages, suggesting the importance of exhumation during initiation of subduction and/or the subduction of a young slab. Based on the frequent occurrence of serpentinite bodies around eclogites, Hermann et al. (2000) suggested that the serpentinite, which may originate at continental margins or slow-spreading ridges, is essential in the exhumation of OC and that special conditions are needed for exhumation to occur.

Penniston-Dorland et al. (2015) discounted preferential exhumation and instead suggested that thermal models are incorrect due to exclusion of certain heat sources, causing the model averages to be colder than the average of the observed rock record. An outstanding question then is whether the disagreement between the metamorphic rock record and the thermal models results from inaccurate thermal models or from preferential exhumation of rocks from warmer subduction settings. In this paper we perform a systematic comparison between thermal model predictions for the subducting OC and the rock record. We show that updated models from Wada and Wang (2009), which include shear heating along the top of the slab below the forearc, predict somewhat warmer conditions than van Keken et al. (2011) but remain significantly colder than the rock record. We then add arbitrary heat sources along the slab surface to make the model predictions conform with the rock record and show that these new models violate independent geophysical and geochemical observations. We conclude that the discrepancy between the rock record and thermal models is best explained by preferential exhumation of subducted mafic rock from warm subduction settings where higher temperatures lead to more efficient thermally activated creep and fluid-induced buoyancy and mobility to facilitate exhumation.

2. Methods

We developed new finite element models that predict the thermal structure of subduction zones by closely following the approaches in Wada and Wang (2009) and van Keken et al. (2011). Wada and Wang (2009) provided 17 models for specific cross sections across subduction zones with varying thermal conditions. van Keken et al. (2011) provided a minor update to the 56 models in Syracuse et al. (2010) that were developed to capture the average conditions across 800 km wide swaths along most of Earth's subduction zones.

The modeling approach applied here is similar. We assume a kinematic slab surface with a geometry that is constrained from seismicity and local observations (see, e.g., Syracuse & Abers, 2006; Figure 1a). The models assume constant convergence velocity with a magnitude that is based on observed convergence velocities at the trench projected onto the cross section. The velocity in the slab is either kinematically prescribed (van Keken et al., 2011) or determined by a separate solution of the Stokes equation in the slab assuming constant viscosity (Wada & Wang, 2009). The thermal structure of the slab that is prescribed at the trench side boundary is based on the age of the slab at the trench. We assume a rigid crust in the overriding plate and a dynamic wedge with a rheology that is based on the deformation of olivine by dislocation creep (Karato & Wu, 1993). We assume that the slab is decoupled from the overriding plate to a depth of 75 km (Wada & Wang, 2009) or 80 km (van Keken et al., 2011). This leads to the formation of a cold corner in the mantle wedge below the forearc.

Within the dynamic wedge we solve the incompressible Boussinesq equations for conservation of mass

$$\nabla \cdot \mathbf{v} = 0 \tag{1}$$

and conservation of momentum

$$-\nabla P + \nabla \cdot \underline{\underline{\sigma}} = \mathbf{0}, \tag{2}$$

where $\mathbf{v}$ is the velocity vector, P is dynamical pressure, and $\underline{\underline{\sigma}}$ is the deviatoric stress tensor given by

$$\underline{\underline{\sigma}} = 2\eta\underline{\underline{\dot{\epsilon}}}, \tag{3}$$

where η is the dynamic viscosity (that depends on both temperature and strain rate) and $\underline{\underline{\dot{\epsilon}}}$ is the deviatoric strain-rate tensor with components

$$\underline{\underline{\dot{\epsilon}}}_{ij} = \frac{1}{2}\left(\frac{\partial v_i}{\partial x_j} + \frac{\partial v_j}{\partial x_i}\right), \tag{4}$$

where v_i are the components of the velocity vector $\mathbf{v}$ and x_i are the coordinates. We neglect thermal buoyancy as the principal buoyancy force driving the dynamics is represented by the kinematic boundary condition. The flow in the mantle wedge is purely driven by the drag of the slab (imposed as a velocity boundary condition downdip from the coupling point).

In van Keken et al. (2011), the thermal evolution of the subduction zone is computed by solving the time-dependent heat equation for the entire domain:

$$\rho c_p \left(\frac{\partial T}{\partial t} + \mathbf{v} \cdot \nabla T\right) = \nabla \cdot (k\nabla T) + Q, \tag{5}$$

where ρ is density, c_p is specific heat, T is temperature, t is time, k is thermal conductivity, and Q is internal heating. At each time step, the viscosity is computed based on the updated temperature and velocity, and the Stokes equations (1) and (2) are solved before the next time step of the heat equation. In the models of Wada and Wang (2009), steady state heat transfer is assumed (i.e., without the time derivative of temperature in equation (5) and viscosity is computed iteratively in a fashion similar to that of van Keken et al. (2011) until prescribed convergence criteria are met.

In this paper, the internal heating is the sum of radiogenic heat production Q_H and shear heating Q_{sh} along the subduction interface down to the slab-wedge coupling point (Figure 1). The shear heating is composed of two parts. Frictional heating occurs along the shallow, cold, and often seismogenic segment. This heating term is proportional to slab velocity and shear stress along the fault. Viscous heating occurs further downdip until the slab mantle coupling point. This term is either calculated from the product of shear stress and strain rate or imposed as a simple linear decrease as further discussed below.

Our models ignore possible redistribution of heat by vigorous hydrothermal circulation within the shallow OC that may result in slightly cooler conditions (e.g., Spinelli & Wang, 2009). This effect can be locally important for some segments of very young and warm subducting plates but is unlikely to be important for the majority of subduction zones.

For the models presented here, we made a few changes to the model assumptions of Wada and Wang (2009) to be closer to the assumptions of van Keken et al. (2011). Most importantly, we chose a uniform mantle potential temperature of 1421.5 °C, which corresponds to the potential temperature used in the GDH1 plate cooling model (Stein & Stein, 1992). This choice for potential temperature is at the high end of the range determined from geochemistry or seismology (Dalton et al., 2014; Herzberg et al., 2007). Logically, the use of a lower potential temperature would lead to a stronger discrepancy between the rock record and the thermal models. We refer to the modified models from Wada and Wang (2009) as WW09m. We compare the steady state WW09m models to time-dependent models similar to those presented in van Keken et al. (2011). The models in van Keken et al. (2011) were evaluated at 20 Myr after subduction initiation, except for a few cases with

low convergence speed that were evolved to 40 Myr. This time integration is in general long enough for the models to reach a quasi steady state in the slab thermal structure, but, just to be sure, all models presented here are integrated to 60 Myr. We refer to the models with this longer time integration as vK11m. The model equations are solved using independent high-resolution finite element methods that show excellent agreement in a benchmark for subduction zone thermal models (van Keken et al., 2008). We provide further details of the finite element modeling in the appendix. Parameters such as convergence speed and age of the slab for the models are provided in Table A1.

3. Results

We first compare the vK11m models to the rock record. It is not uncommon in petrology papers to represent the thermal structure of subduction zones using just the temperature as a function of pressure at the top of the slab (e.g., Hacker, 2008; Penniston-Dorland et al., 2015). The top of the slab includes sediments and is not necessarily the top of the igneous OC. Because mafic rocks are generally exhumed from the subducting OC (which is a volume) and not from the top of the slab (which is a surface), we focus explicitly on the interior of the OC. We divide this subducting crust into seven 1 km thick layers (assuming an average OC thickness of 7 km). The thermal structure at the top of the crust is represented by the path in the middle of the topmost layer that is centered 0.5 km below the top of the pillow basalts. The thermal structure at the bottom of the OC is represented by the layer that is centered 0.5 km above the slab Moho. We also show the average temperature in the crust, which is simply the depth-averaged temperature across the seven layers.

The average crustal temperature structure is significantly different from that at the top of the slab, particularly when the slab comes into contact with the hot mantle wedge below the arc and backarc, or when heat sources at the top of the slab, such as frictional heating, are added. One should therefore avoid using just the PT path at the top of the slab when comparing models to the exhumed rock record.

Figure 3 compares the temperature at the top and the bottom of the OC (frame a) and the average crustal temperature (frame b) to the rock record. The thin orange line represents the average of the temperature at the top of the slab over all 56 models. The difference between this curve and the SPD15p average is, not surprisingly, quite similar to the difference found between the rock record and the average of the models of van Keken et al. (2011) as discussed in Penniston-Dorland et al. (2015). Below the forearc the model average is 200–300 °C lower than the rock PT average but the model and rock averages are nearly identical below the arc.

The more appropriate comparison between the rock record and the crustal average (thick orange line) shows that the model crust remains significantly colder than the rock record even below the arc. The main reason is that the conduction of heat into the crust from the hot overlying wedge is slow and less efficient than the advection of the cold slab. Heating of the deeper crust is delayed in particular for fast subduction zones. This effect is further illustrated by the large difference between the PT paths for top and bottom of the OC (Figure 3a), which indicates strong temperature gradients. The discrepancy between the rock and model averages is even larger than suggested by Penniston-Dorland et al. (2015).

3.1. Effect of Reasonable Shear Heating Along the Top of the Slab

Shear heating along the top of the shallow slab was not included in the models of van Keken et al. (2011), in contrast to modeling by other workers (e.g., Kneller et al., 2007; Peacock & Wang, 1999; van Keken et al., 2002; Wada & Wang, 2009), Shear heating Q_{sh} in subduction zones arises from the dissipation of mechanical work along the plate interface and by dissipation during viscous deformation and can be added mathematically to the right-hand side of the heat equation (5).

One reason for assuming $Q_{sh} = 0$ in van Keken et al. 2011 was that the calculated effect is generally small and does not significantly affect the mantle wedge thermal structure below the arc (e.g., Kneller et al., 2007). We will demonstrate below that the effect on the forearc thermal structure is also small. The second reason was that the Boussinesq equations, which arise from a simplification of the equations for flow in a compressible anelastic liquid medium and explicitly assume that the dissipation number $Di = 0$, where $Di = \alpha g h / c_p$, with α thermal expansivity and h a typical length scale, such as the depth of the convecting layer. Shear heating, thermal effects of phase changes, and adiabatic compression and decompression all scale with this number (Jarvis & McKenzie, 1980; King et al., 2010; Schubert et al., 2001).
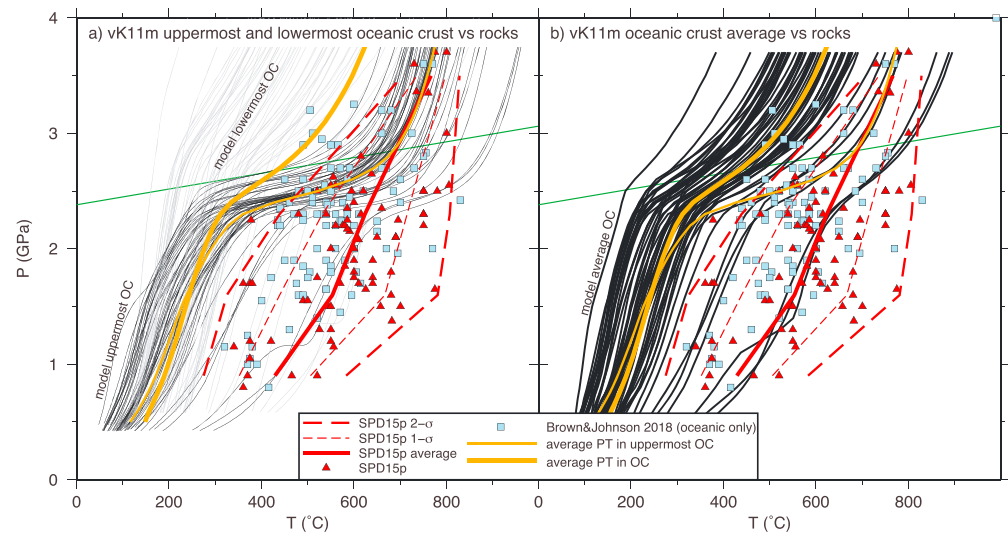
Figure 3. Comparison between thermal models of vK11m (without shear heating) and the rock record (as in Figure 2). (a) Slab PT paths for the uppermost OC (0.5 km below top of slab; bold black lines) and lowermost crust (6.5 km into the OC; gray lines). (b) Average slab PT paths in the oceanic crust in each model. The average temperature in the top of the crust in all 56 models is represented by the thinner orange line. The thicker orange line indicates the average temperature in the crust in all 56 models. Because blueschists and eclogites presumably are exhumed from all levels in the crust, it is appropriate to use the full crustal average. Penniston-Dorland et al. (2015) used the slab top average only. The difference between the average uppermost OC and the rock average increases from ~200 °C at shallow depths to ~300 °C at 2 GPa before disappearing under UHP conditions (as was shown in Figure 7 of Penniston-Dorland et al., 2015). The crustal averages remain significantly cooler than the average PT path of the rock record for $P > 2.7$ GPa. The green line indicates the transition from HP to UHP rocks (Bose & Ganguly, 1995), which corresponds closely to the depth where the slab couples to the overriding mantle wedge and the slab tops undergo rapid warming. PT = pressure-temperature; OC = oceanic crust; HP = high pressure; UHP = ultrahigh pressure.

To be fully consistent, one should only study the effects of shear heating in models that also take into account the other terms that scale with *Di*. This can be achieved using fully compressible models (e.g., Christensen & Yuen, 1985; Jarvis & McKenzie, 1980; King et al., 2010). Alternatively, the extended Boussinesq approximation can be used. This approximation assumes finite *Di* in the heat equation but retains the incompressible form of the mass-conservation equations (Arredondo & Billen, 2017; Čížková & Bina, 2013; Lee & King, 2009).

There are some studies where high shear heating was added to Boussinesq models that may have caused artificial heating. Bodri and Bodri (1978) added viscous dissipation to the wedge in a kinematically driven Boussinesq model until the temperature reached 1700 K below the arc. Their thermal models seem to suffer from high local shear heating (although it is possible that relatively low resolution is to blame for what appear to be artifacts in their thermal models where very high temperatures occur in a spot in the shallow mantle). Kneller et al. (2007) added viscous dissipation in the wedge as part of a parameter sensitivity study. They found that, due to the low viscosity in the hot mantle wedge, shear heating was negligible and had little effect on the thermal structure there. The viscous dissipation in the cold corner of the wedge caused an increase of 100–150 °C in the cold forearc corner of wedge, which may be an artifact of adding this nonconservative heat source when stresses are high. Peacock et al. (1994) added significant frictional heating to the top of the slab by assuming a constant shear stress of up to 100 MPa to great depth in order to explain melting of the subducting OC. It was later found that this was unnecessary and that the use of a realistic olivine rheology in the wedge explains melting of the hydrated OC below the arc (van Keken et al., 2002).

Despite these caveats, it is appropriate for these long-term subduction zone models to include the heat that is produced by the mechanical dissipation along the plate interface. The motion of the shallow and *brittle* part of the plate interface can be frictional sliding along the contact surface or cataclastic shear of a fault zone of finite thickness and can be in the form of repeated seismic slip, creep events, or steady creep that is accompanied by small earthquakes (Wang & Bilek, 2014). The resultant spatiotemporally averaged energy dissipation rate Q_f is proportional to the long-term frictional stress τ and the subduction rate V. The frictional

stress is commonly obtained using a static friction law, which in subduction zone models leads to

$$Q_f = \mu' P_l V \delta(x_{\text{interface}}), \tag{6}$$

where μ' is the effective friction coefficient and $P_l = \rho_m g z$ is the lithostatic pressure that is used to approximate normal stress across the fault (with ρ_m the density of the mantle, g the gravitational acceleration, and z depth). The δ function in (6) has dimension m^{-1} with the property

$$\int \delta(x_{\text{interface}}) d\Omega = 1, \tag{7}$$

where $x_{\text{interface}}$ is the location of the plate interface and Ω is the spatial domain.

The assumed effective friction coefficient is a free parameter. Inferences based on the force balance in the forearc (e.g., Lamb, 2006; Wang & He, 1999) and surface heat flow observations (Gao & Wang, 2014, 2017; Wang et al., 1995) indicate that subduction faults are exceedingly weak, with μ' typically less than 0.05. In this formulation, any effects of pore pressure on the fault are incorporated in μ'. The value of μ' used in frictional heating calculations represents the strength of the subduction zone when it is in motion. Because of velocity weakening or dynamic weakening during seismic slip, for highly seismogenic megathrusts the μ' value relevant to frictional heating is slightly less than the actual static strength of the fault, as explained by Gao and Wang (2014). For the purpose of this work, it is convenient and appropriate to continue the practice of Wada and Wang (2009) to use a representative value of $\mu' = 0.03$ and to define the downdip end of the frictional regime using the observed termination of interface seismicity.

The deeper and *ductile* part of the interface exhibits viscous shear (Shimamoto & Noda, 2014) and the viscous energy dissipation is $Q_d = \underline{\underline{\tau}} : \underline{\underline{\dot{\epsilon}}}$. Wada and Wang (2009) assumed that the viscous coupling occurs from the downdip end of the frictional regime down to a depth of 75 km and used a quartz diorite rheology in a thin shear zone to compute Q_d. Because of increasing temperature with increasing depth, Q_d drops quickly from its peak at the frictional-viscous transition and becomes negligibly small before 75 km depth is reached.

We provide a direct comparison between the models WW09m with our estimate for reasonable amounts of shear heating $\mu' = 0.03$ and those without. We also compare these two suites of models to vK11m. The comparison of WW09m with and without shear heating provides a direct and clean estimate of the effects of shear heating in subduction zones. Figure 4 shows the full comparison in frames (a) through (c). Figures 4b and 4c show that the WW09m models—like the vK11m models—are on average significantly colder than the rock record and that the assumed amount of shear heating does not make a significant difference. Table 1 quantifies the average differences as a function of pressure between the vK11m (without shear heating) and WW09m models (with and without shear heating). Between 1 and 2 GPa, the vK11m models are about 25 °C cooler than the WW09m models without shear heating, primarily because the vK11m models have on average older incoming plate ages and higher convergence speeds. The effect of shear heating is to increase the average OC temperature by less than 50 °C, which is significantly less than the 200–300 °C difference between the models of van Keken et al. (2011) and the rock record.

Figures 4d–4f show the same models as 4a–4c but only for young oceanic lithosphere. This comparison shows that the warm conditions in young oceanic lithosphere are similar to those seen in the rock record, suggesting that preferential exhumation of young oceanic lithosphere may in part explain the model-rock discrepancy. The WW09m models with shear heating (Figure 4f) seem to lie well within the limits of the rock record although some of the warmest conditions for $P < 2.5$ GPa that are seen in the rock record are not predicted by any of the models.

Based on previous analytical work (e.g., Molnar et al., 1979), Kirby et al. (1991) introduced the *thermal parameter* to provide a simple quantification of the thermal structure of subduction zones. The subduction zone thermal parameter ϕ is the product of age, convergence speed, and sin Δ, where Δ is the dip of the subduction zone. Larger ϕ denotes cooler material that is advected more efficiently to depth than with smaller ϕ. Because exhumed rocks provide no record of the dip angle of the subducting slab from they were exhumed and slab dip varies with depth, we will use the modified thermal parameter ϕ' instead. This is simply the age of the oceanic lithosphere at the trench times the convergence speed. We show that the model-predicted crustal PT conditions of slow and/or young slabs with small ϕ' compare more favorably to the rock record (Figures 4g–4i) although we note that some of the hottest conditions below 2.7 GPa that are observed in the rock record are not reached by these models.

Table 1
Average Oceanic Crust Temperature for vK11m (No Shear Heating) and WW09m (With and Without Shear Heating)

		T (°C)	
		WW09m	
P (GPa)	vK11m	$\mu' = 0$	$\mu' = 0.03$
0.5	146	186	201
1.0	197	231	265
1.5	234	262	305
2.0	274	300	341
2.5	367	473	503

Note. The WW09m models without shear heating are slightly warmer than vK11m because the average thermal parameter is higher in those models. The larger relative difference at 2.5 GPa is due to the assumption of a shallower slab-wedge coupling point in WW09m.

To better illustrate the range of model-predicted PT conditions in the subducting crust, we randomly sample 200 points along the seven OC PT paths of all WW09m models (Figure 5). The sample selection is made by randomly picking a number for the subduction zone (1 to 17), a depth within the OC (0.5 to 6.5 km), and a pressure (between 0.8 and 3.7 GPa, the same pressure range as that of the rocks in SPD15p).

The correlation between age and thermal structure (Figure 5b) is stronger than that between thermal structure and velocity (Figure 5a) or ϕ' (Figure 5c). As was suggested in Figure 4, models with a young incoming oceanic lithosphere (with age ≤30 Ma) or with modest thermal parameter (ϕ' ≤1,000 km) are most similar to the rock record.

3.2. Other Heat Sources That May Change the Thermal Structure of the OC Below the Forearc

Before we turn to a more qualitative discussion of how the thermal models and exhumed rock record may be reconciled, we test the hypothesis provided in Penniston-Dorland et al. (2015) that the exhumed rocks represent the average thermal structure of the subducting crust and that the low temperatures predicted in the models are an artifact of neglecting certain heat sources.

Above we showed that reasonable values for shear heating alone cannot explain the discrepancy between models and rock record. Other mechanisms that could help warm up the crust below the forearc are fluid migration and solid-solid phase changes.

Downdip of the slab-wedge coupling point, the temperature of the crust increases significantly (Figure 1) and fluid production by metamorphic dehydration reactions is predicted to be efficient, leading to fluxing of the overlying mantle wedge with fluids and arc magmatism (e.g., Schmidt & Poli, 1998; Tatsumi, 1986; van Keken et al., 2011). These free fluids may also lead to conditions that enhance intermediate-depth seismicity (e.g., Abers et al., 2013; Hacker et al., 2003; van Keken et al., 2012).

Fluid flow affecting exhumed rock is evident from geochemistry (e.g., Bebout & Penniston-Dorland, 2016; Penniston-Dorland et al., 2012). A strong reduction in P wave speed in the crust of some slabs at depths of 50–100 km has been interpreted to reflect the presence of up to 1 vol % aqueous fluids (Shiina et al., 2013; Shiina et al., 2017). A fraction of these fluids could, instead of fluxing the mantle wedge, flow updip through the OC and carry some heat to the cooler forearc. This is a transport path supported by dynamical modeling (Wilson et al., 2014). Nevertheless, the thermal effect of fluid migration on the cooler rocks below the forearc is expected to be small given the relatively small volume of the fluids and their modest heat capacity.

Solid-solid phase transitions and mineral dehydration reactions change the temperature of the slab due to latent heat effects, which can be both positive and negative. Chemia et al. (2015) provided a comprehensive study of the thermal effects of metamorphic devolatilization reactions in the subducting slab by a perturbation analysis. Their calculations suggest ~50 °C warming of the subducting sediments and OC beneath the forearc by metamorphic reactions and a cooling of similar magnitude in the harzburgitic mantle. The effects of the migration of fluids away from where they are produced counteracts the thermal effects of the
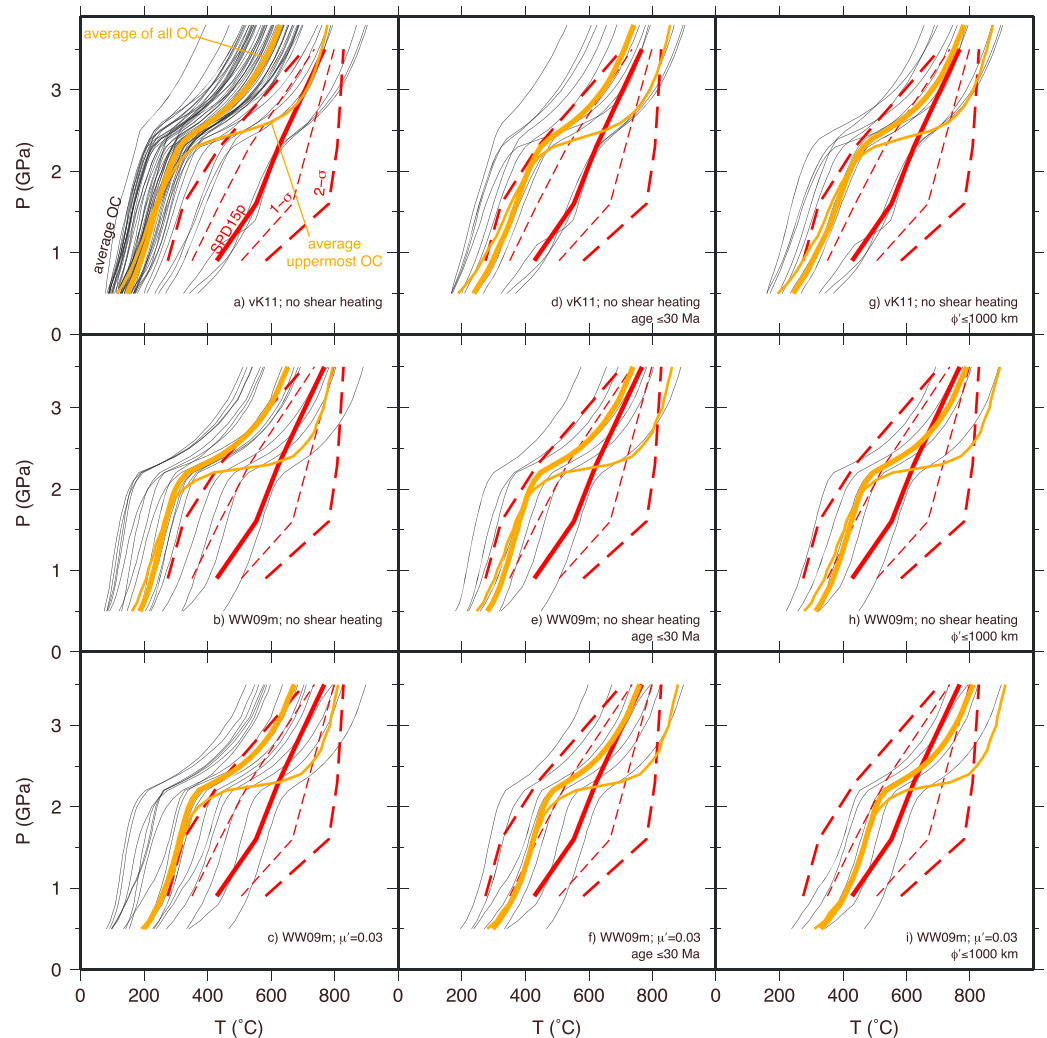
Figure 4. Comparison of models vK11m (without shear heating), WW09m (with and without shear heating), and the rock record. (a) As Figure 3b with average temperature of OC indicated by the black lines; the average over all models for the uppermost crust by the thinner orange line; the average of the entire OC by the thick orange line; and the SPD15p average and 1 and 2σ standard deviations by red lines. (b) As in (a) but for the 17 models of WW09m without shear heating. (c) As in (b) but with reasonable shear heating using $\mu' = 0.03$. (d–f) As in (a)–(c) but only for those models that have an incoming slab age of $\leq$30 Ma. (g–i) As in (a)–(c) but only for those models that have modified thermal parameter $\phi' \leq$1,000 km. The ϕ' is the age of the incoming slab times the convergence speed. OC = oceanic crust.

metamorphic reactions. The resulting overall effect on the thermal structure of the crust is therefore estimated to be rather small.

The updip advection of warmer material from greater depth along the subduction interface could effectively heat the slab surface, such as shown in the models with a forced subduction zone channel of Gerya et al. (2002). Penniston-Dorland et al. (2015) showed in their Figure 7 that such models on average are about 100–150 °C warmer than the global average of Syracuse et al. (2010), which by itself is still insufficient to explain the rock-model discrepancy.

3.3. Models With Arbitrary Heat Sources That Match the Rock Record

Even though the magnitudes of *known* heat sources in the slab below the forearc are small, we can arbitrarily add *unknown* heat sources with a magnitude such that the models predict temperature conditions that are the same as in the rock record. In constructing the shape of heating function we take into account that the difference between the average of the rock record and that of the models increases with pressure from 1 GPa until it reaches a maximum just above 2 GPa (Figures 3 and 4). That suggests that the magnitude of the
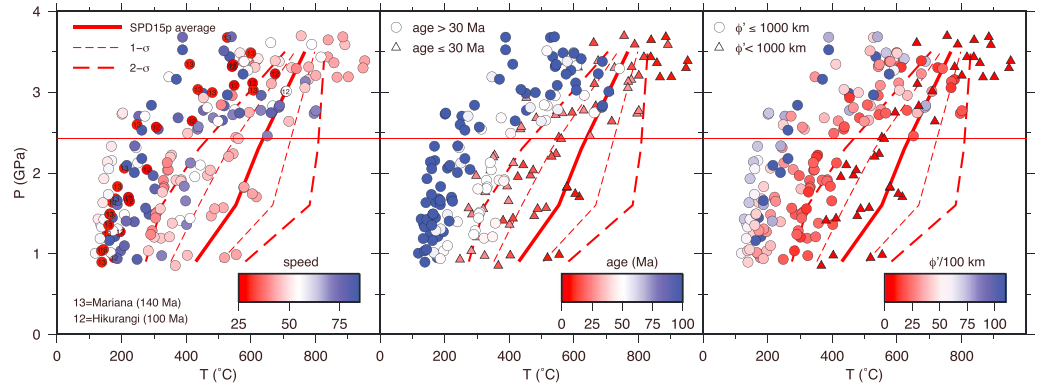
Figure 5. Random sampling from the crust thermal structure predicted by WW09m (with $\mu' = 0.03$). Samples are randomly picked within the pressure range 0.8–3.7 GPa, within the subducting crust, and within the 17 models. (a) Symbol colors indicate the convergence speed. Lower speed tends to yield warmer conditions, but important exceptions occur for slow moving old oceanic lithosphere (such as those in the Mariana and Hikurangi subduction zones). (b) Same as (a) but color coding and symbol shape are for age of the incoming lithosphere. The thermal conditions trend warmer for younger oceanic lithosphere. (c) Same as (b) but for modified thermal parameter ϕ'. While the trend of temperature with ϕ' is weaker than that with age alone, most of the samples for $\phi' \leq 1{,}000$ fall within the pressure-temperature conditions of the rock record.

arbitrary heat sources should first increase with depth and then decrease from a maximum above 2 GPa to explain the rock record.

Figure 6 shows the shear heating along the top of the crust in WW09m. The thermal effect of this shear heating depends on the effective coefficient of friction μ' (assumed to be 0.03 here) and the convergence speed V. In addition, the dip of the slab plays a role because shallowly dipping slabs tend to have a greater shear heating effect than steeply dipping slabs. The average of the shear heating over these 17 models is shown in the red curve. We approximate this by a depth-dependent arbitrary heating function $Q_{stylized}$ of the form

$$
Q_{\text{stylized}} = \begin{cases} 0.024 V P_l z \ : \ z \leq z_{30} \\ 0.024 V P_l (z_{80} - z)/(z_{80} - z_{30}) \ : \ z > z_{30} \ \text{and} \ z \leq z_{80} \\ 0 \ : \ z > z_{80} \end{cases} \tag{8}
$$

where V is convergence speed, P_l is an approximation of lithostatic pressure as introduced before, z is depth, $z_{30} = 30$ km, and $z_{80} = 80$ km. Note that this assumption effectively redistributes some of the heating in WW09m from shallow depth to greater depth with this assumption.

We modify the heating term in (5) to

$$
Q = Q_H + f_{\text{arbi}} Q_{\text{stylized}} \delta(x_{\text{interface}}), \tag{9}
$$

where f_{arbi} is an arbitrary constant that we vary until we find a reasonable match between the models and the rock record using the models of vK11m.

We find that using a factor $f_{\text{arbi}} = 7$ leads to a similar predicted average temperature for the crust similar to that of the SPD15p rock record. If this heating term were due to shear heating alone, then an effective friction coefficient $\mu' = 0.21$ is implied.

Figure 7a shows the temperature in the uppermost OC (thick black lines) and lowermost OC (thinner black lines) in comparison to the rock record—similar to Figure 3a, but for the vK11m models with $f_{\text{arbi}} = 7$. Figure 7b shows the difference in average of temperature between these new warmer models and the rock record as a function of f_{arbi}. Note that the difference between $f_{\text{arbi}} = 0$ and $f_{\text{arbi}} = 1$, where the latter corresponds to heating as in WW09m with $\mu' = 0.03$, is similar to that between the WW09m models with and without shear heating.

Figure 8 shows the PT conditions for 200 random samples pulled from the model OC and are compared to SPD15p. In addition to the similarity in averages, we find similarity in spread as well, with most samples contained within the 2σ lines. Outliers tend to be hotter than the rock record in particular for models with young oceanic lithosphere.
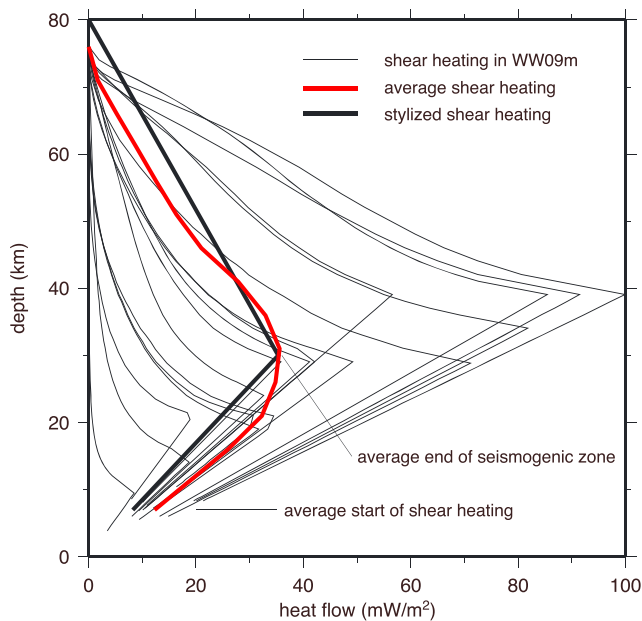
Figure 6. Shear heating along the top of the crust in WW09m is shown in the thin black lines. The downdip limit of the seismogenic zone defines the maxima of these curves and has an average depth of 30 km. The average depth where shear heating starts is 7 km. The average shear heating in these models is shown by the red curve. The bold black curve results in the same amount of integrated shear heating and functions as our stylized averaged shear heating for new models that will be used to try to match the rock record. This functional description for shear heating along the fault is a simplification of that obtained by more advanced models that show a more gradual transition between the two mechanisms (Gao & Wang, 2014; Shimamoto & Noda, 2014), but the simpler model is consistent with that used in Wada and Wang (2009) and suffices for the purposes of this paper.

Even though adding high arbitrary heat to the models produces good agreement between the models and the rock record, we do not know of any heat source that could physically produce the heating needed as discussed above. This comparison is provided simply to see what is necessary to reproduce the rock record with our current modeling approach. These new arbitrarily hot models are compared to independent geochemical and geophysical observations below.

3.4. Comparison of vK11m With a High Arbitrary Heat Source to Independent Observations

Heat flow observations. We first determine the effects of the arbitrary heating modes on the surface heat flow. Because the crust below the forearc is much hotter in the arbitrary heating models, the forearc itself is also significantly warmer. This leads to a significantly higher heat flow at the surface. For the models without heating along the plate interface (Figure 9a), heat flow drops at the trench to a minimum over the forearc and then gradually increases toward the arc. The models tend to converge to an average heat flow of about 65 mW/m^2, which is the average continental heat flow assumed in these models. The globally averaged heat flow in vK11m with $f_{arbi} = 7$ is more than twice that of the models with $f_{arbi} = 0$ and significantly higher than typical heat flow values over the forearc (Wada & Wang, 2009, and references therein). Figure 9c shows the global average in vK11m as a function of f_{arbi} in comparison to the average heat flow predicted by WW09m without shear heating and with a reasonable amount of shear heating (proportional to $\mu' = 0.03$). The heat flow in WW09m tends to be higher above the shallow forearc compared to vK11m because of differences in model assumptions, including a more shallowly dipping slab surface in the shallow forearc, a higher average thermal parameter, and the treatment of the thermal effect of sedimentation before subduction.

We further test whether heat flow measurements would allow high arbitrary heating by using two well-studied end-member margins. Figure 10 shows models that were constructed specifically for the Cascadia margin
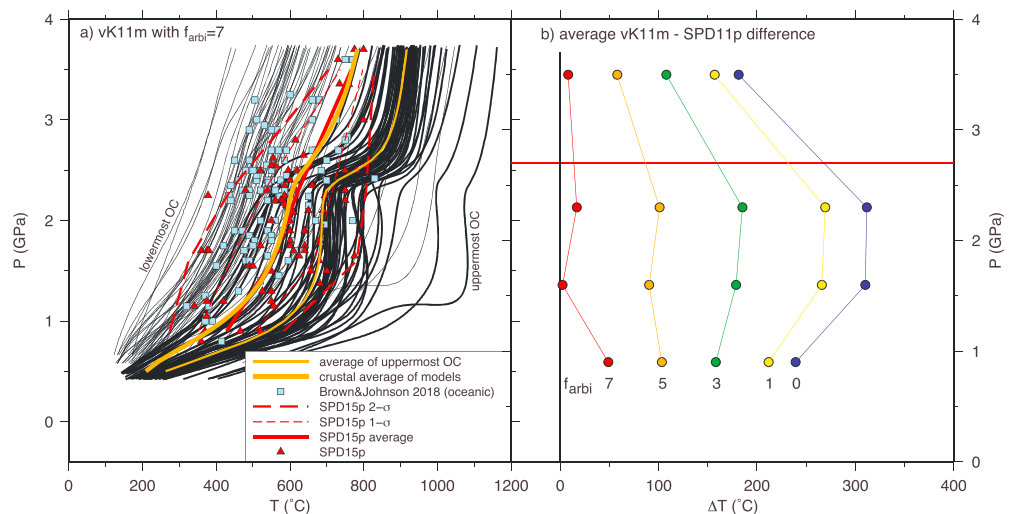

Figure 7. Results of adding an arbitrary heating term $f_{arbi}Q_{stylized}$ to the heating term (7) in the models of van Keken et al. (2011). (a) vK11m model comparison with the rock record as in Figure 3a but with added heating $f_{arbi}Q_{stylized}$ with $f_{arbi} = 7$. The average oceanic crustal temperatures predicted from the models (thick orange line) is nearly identical to the average from SPD15p (thick red line). (b) Difference between vK11m model average and the SPD15p average as a function of f_{arbi}. OC = oceanic crust.
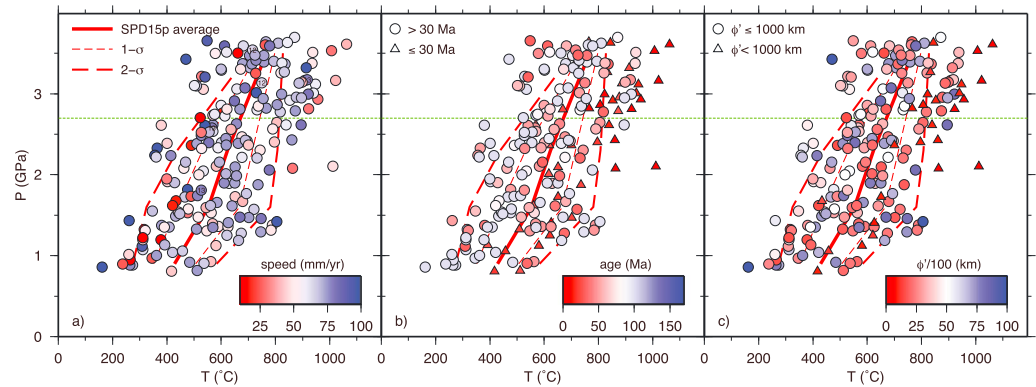
Figure 8. Random sampling of the oceanic crust thermal structure as in Figure 5 but for vK11m models with arbitrary heating with $f_{arbi} = 7$ with symbols colored by speed (frame a), age (frame b), and modified thermal parameter (frame c).
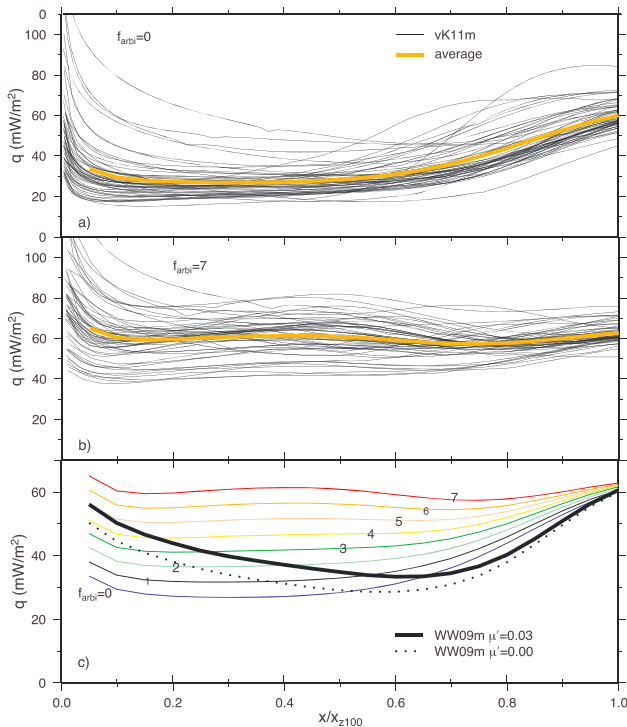

Figure 9. Heat flow over the forearc plotted as function of the nondimensional coordinate x/x_{z100}, where x_{z100} is the distance from the trench where the top of the oceanic crust is at 100 km depth. (a) Heat flow over the 56 models of vK11m (without shear heating) in black with the global average in the thick orange line. The divots in individual curves (e.g., in the top curve at $x/x_{z100} = 0.38$) are due to the change in model topography at the coastline, because we assumed an upper surface in the models that consists of two linear segments with the first rising from trench to coastline and the second at a constant depth of 0 km. (b) Same but for the 56 models of vK11m with the high arbitrary heating ($f_{arbi} = 7$). (c) Comparison of the global averages of vK11m as a function of f_{arbi}. We also show the global average of the 17 models of WW09m without and with shear heating ($\mu' = 0.03$).

(in a cross section below the CAFE seismic experiment as discussed in Abers et al., 2013) and for Tohoku (cross section T18 from van Keken et al., 2012). For this particular Tohoku model we assume that the downdip limit of the seismogenic zone is at 40 km depth, while we acknowledge that several indicators suggest the seismogenic zone may be deeper by yet another 10 to 20 km (Asano et al., 2011; Igarashi et al., 2001). The heat flow over Cascadia is low in part because of the relatively unradiogenic, basaltic Siletzia terrane accreted below the forearc (e.g., Wells et al., 2014). The mafic nature of this crust causes a significant reduction in heat production compared to average continental crust. For this specific CAFE cross section we assumed zero heat production in the upper crust in the forearc (as in Wada & Wang, 2009; Wada et al., 2008).

We compare the models with the same modified heating term (9) and f_{arbi} ranging from 0 to 7 to the local heat flow within 100 km distance from each profile (Figure 10). In the case of Tohoku we show the average heat flow for the entire Tohoku margin as well. In both profiles, the observed forearc heat flow is generally low and increases abruptly close to the arc (which in these two models is where the slab is at about 100 km depth). The high and scattered heat flow is due to magma migration in the mantle wedge and crustal processes that are not taken into account in our models. The Tohoku heat flow observations may allow for slightly higher arbitrary heating than $f_{arbi} = 1$, but it is difficult to satisfy the observed heat flow over Cascadia with significant heating along the top of the slab below the forearc. The heat flow data alone allow us to reject the hypothesis that present-day OC below the forearc has a thermal structure similar to that suggested by the rock record.

Slab surface temperature beneath the arc. In our models with high arbitrary heating, the top of the OC is significantly hotter than the crustal average in all subduction zones and, on average, the temperature at the top of the slab increases by ~150 °C compared to the models without arbitrary heating (see, e.g., Figures 3a and 7a). The differences in slab surface temperature between models with $f_{arbi} = 0$ and 7 decrease with depth beneath the arc (e.g., the difference is 174 °C at 3 GPa and 132 °C at 3.8 GPa). This means that the temperature difference between high arbitrary and low arbitrary heating models is partially overprinted by the corner flow.
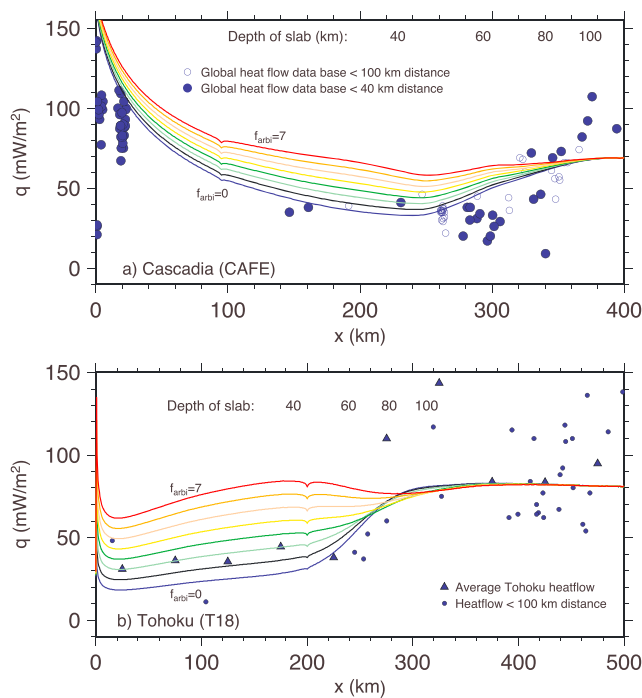
Figure 10. Heat flow over the forearc and arc in (a) Cascadia (CAFE profile of Abers et al., 2013) and (b) Tohoku (T18 profile of van Keken et al., 2012) compared to model predictions of vK11m with variable arbitrary heating. Heat flow values for Cascadia are from the global heat flow data base compiled by the International Heat Flow Commission (Pollack et al., 1993; see also http://www.geophysik.rwth-aachen.de/IHFC/heatflow.html). Heat flow data for Tohoku are from Tanaka et al. (2004). Because the heat flow data are fairly sparse over this cross section, we added the average heat flow in 50 km bins across the Tohoku margin.

We can compare the model predications for slab surface temperatures beneath the arc to independent determinations from geochemistry. Slab surface temperatures have been constrained with experimental work on the melting of sediments (e.g., Hermann & Spandler, 2007; Johnson & Plank, 1999; Skora & Blundy, 2010) and thermobarometry, such as that based on H_2O/Ce in melt inclusions that correlate inversely with slab surface temperature (e.g., Plank et al., 2009). Early evidence for sediment melting beneath arcs (Johnson & Plank, 1999) suggested that the sediment melt signature found in arc magmas indicate slab surface temperatures ~800 °C. This was at odds with the geodynamical models of that time that assumed isoviscous wedge rheology (see review in Peacock, 1996) and predicted much cooler slab surface temperatures below the arc. The evidence for sediment melting is in good agreement, however, with the models that result from using a more realistic mantle rheology based on olivine creep laws as used in this paper (Figure 4) and as discussed in van Keken et al. (2002). Cooper et al. (2012) demonstrated a correlation between the temperature at the top of the slab beneath a number of arcs as predicted by van Keken et al. (2011) and slab surface temperatures determined from the H_2O/Ce geothermometer. In Figure 11 we closely reproduce their results using the vK11m models without shear heating (solid circles). The green squares show the slab surface temperatures taken from van Keken et al. (2011). Our present results tend to be a little cooler because of the longer integration time assumed. The red triangles show the slab surface temperature beneath the arc for vK11m models with high arbitrary heating (f_{arbi} = 7). The strong agreement between the models without shear heating and geochemical data disappears for the high arbitrary heating case. The slab temperature is on average 160 °C hotter beneath the arcs, and the models provide a poor fit to the geochemical data. It is clear that the model predictions from the high arbitrary heating case are not compatible with the H_2O/Ce data. Moreover, Hermann and Spandler (2007) showed that the phengite dehydration melting in experiments at subarc temperatures of 950–1000 °C imparts a K_2O/H_2O ratio of 2 to the sediment melt, which, as they noted, is inconsistent with K_2O/H_2O of 0.1–0.5 observed in arcs. As such the high temperatures predicted for the high arbitrary heating model are inconsistent with these observations.

Predicted forearc thermal structure compared to geochemical and seismological observations. The high arbitrary heating case predicts very high temperatures in the slab and forearc mantle for the warm-slab subduction zones, such as Cascadia, which appear inconsistent with geochemical and geophysical observations. Figure 12 shows the predicted mineralogically bound H_2O content and *P* wave speeds for the OC, uppermost slab mantle, and overlying mantle for models with zero and high arbitrary heating in Cascadia, Nicaragua, and Tohoku using the elastic moduli of Abers and Hacker (2016). The figures show bound H_2O and *P* wave speeds along paths that are close to the slab and run parallel to the slab surface. They are straightened for the graphical representation so that the vertical coordinate is depth into the slab (perpendicular to the slab surface) and the horizontal coordinate represents the distance along the top of the slab.

The Cascadia model with f_{arbi} = 0 shows a hydrated mantle wedge down to the coupling point at 80 km depth, a crust that dehydrates at shallower depths, and a 2 km thick layer of serpentinized mantle below the oceanic Moho that extends to just below the volcanic front. This predicts that fluids in the Cascadia arc are sourced from the slab mantle, which is consistent with boron and hydrogen isotopic studies that identify the slab mantle as source for the fluids (Walowski et al., 2015, 2016). The high water content found in the basalts produced in this arc (Plank et al., 2013) requires that hydrated rock is advected to below the region of magma genesis. In the high arbitrary heating case the crust and mantle completely dehydrate before they reach 40 km depth thereby removing the potential for any slab fluids sourcing arc volcanism, which is in clear conflict with the geochemical data. Complete dehydration of the entire crust and slab mantle below the forearc is also predicted for Northern Cascadia (Vancouver Island), Mexico, and Southern Chile.
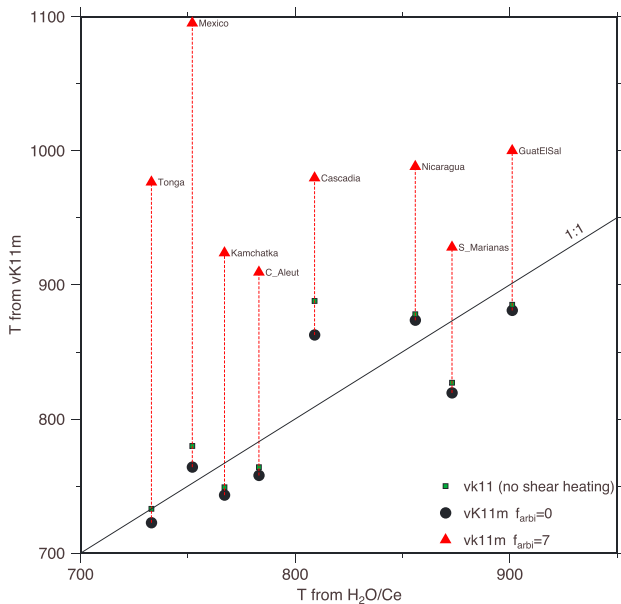
Figure 11. Comparison of slab surface temperature determined from the H_2O/Ce thermometry (Cooper et al., 2012) and slab surface temperature calculated from corresponding models. Green squares are the vK11m data with shorter integration time used in Cooper et al., (2012, their Table 1 and Figure 9). Black circles are from vK11m without shear heating, which show slightly cooler conditions caused by the longer integration time that is assumed. Red triangles are from vK11m with $f_{arbi} = 7$.

Nearly all the vK11m models with high arbitrary heating have a hot forearc mantle with temperatures outside the antigorite stability field in all but a few arcs. This conflicts with seismic observations in warm arcs. For example, the forearc mantle wedge in Cascadia is characterized by low seismic velocities ($\sim$7.2 km/s; see Abers et al., 2017, and references therein) and a nonexistent or possibly inverted Moho (Bostock et al., 2002; Hansen et al., 2016). These seismic characteristics are best explained by a hydrated wedge with abundant serpentine and/or chlorite. Models without shear heating (van Keken et al., 2011) predict that the warm OC in Cascadia releases abundant fluids below the forearc. Abers et al. (2017) calculated that enough time has elapsed that the forearc mantle wedge should be hydrated—and full of antigorite and/or chlorite—and has slow seismic wave speeds, as observed. In contrast, in models with high arbitrary heating (Figure 12, frame a4), the forearc mantle is too hot for antigorite and chlorite to be present and the predicted seismic wave speeds are $\sim$8 km/s, much larger than observed. The temperature effects on P wave speeds are small compared to those of serpentinization for the 200–400 °C variations between these models. Colder subduction zones do not display such low forearc P wave speeds (Abers et al., 2017), and it is difficult to separate temperature effects from those of composition based on seismic wave speeds alone in those regions.

Seismic attenuation provides a stronger constraint on thermal structure. In many arcs it shows that the mantle wedge abruptly transitions from low to high attenuation above where the slab surface reaches 80 km depth (Abers et al., 2006; Nakajima et al., 2013; Rychert et al., 2008). Calculations shown in this paper reveal that the effect is easily reproduced in thermal models without heating along the plate interface but that the addition of high arbitrary heating ($f_{arbi} = 7$) produces attenuation patterns that are inconsistent with observations (Figure 13). Overall, the comparison between models without interface heating (Figure 13c) and those with high arbitrary heating (Figure 13d) clearly shows that the high heating mode eliminates the low attenuation signature of the cold forearc, which is in conflict with the observations.

Implications for global H_2O flux. In the high arbitrary heating models the sediments and uppermost crust are predicted to dehydrate completely before 80 km depth but water is available in the gabbro and upper mantle at subarc depths. The efficient dehydration of the uppermost crust leads to a significant flux of H_2O from the slab below the forearc (Figure 14). Figure 14a is similar to the *Tokyo Subway Map* of van Keken et al. (2011), with slight differences due to the longer integration time in vK11m. The models without shear heating are predicted to produce 3.5×10^8 Tg/Myr between 75 and 100 km depth; this is reduced to 1.5×10^8 Tg/Myr for the high arbitrary heating models. The first estimate is in good agreement with estimates of the global arc loss (3×10^8 Tg/Myr; Wallace, 2005). The second requires twice as much H_2O from arcs as that predicted to leave the slab, posing a mass balance problem.

The predicted transport of H_2O to the deep mantle is strongly affected. van Keken et al. (2011) predicted a present-day return flux to the mantle of 3.4×10^8 Tg/Myr or approximately one ocean mass over the age of the Earth. Taking into account estimates for the secular evolution of the Earth, this is in good agreement with estimates from the recycling of noble gases (Holland & Ballentine, 2006) for the models without shear heating, but not for the high arbitrary heating models that predict a flux past 230 km of nearly three times less (1.3×10^8 Tg/Myr for $f_{arbi} = 7$ versus 3.7×10^8 Tg/Myr for $f_{arbi} = 0$). The return flux estimate from van Keken et al. (2011) is in excellent agreement with independent model estimates from Parai and Mukhopadhyay (2012) who preferred a value of 3.6×10^8 Tg/Myr to maintain a near steady state ocean since the Precambrian. The low return flux in the arbitrary heating models is predicted to increase sea level over the last 540 Myr by $\sim$ 100 m, which is well outside of the range permitted by Phanerozoic sea level reconstructions (see references in Parai & Mukhopadhyay, 2012).

For reference, the models with reasonable shear heating ($f_{arbi} = 1$) predict that the slab crust and mantle undergo minimal additional dehydration below the forearc (less than 1% difference) and only slightly more
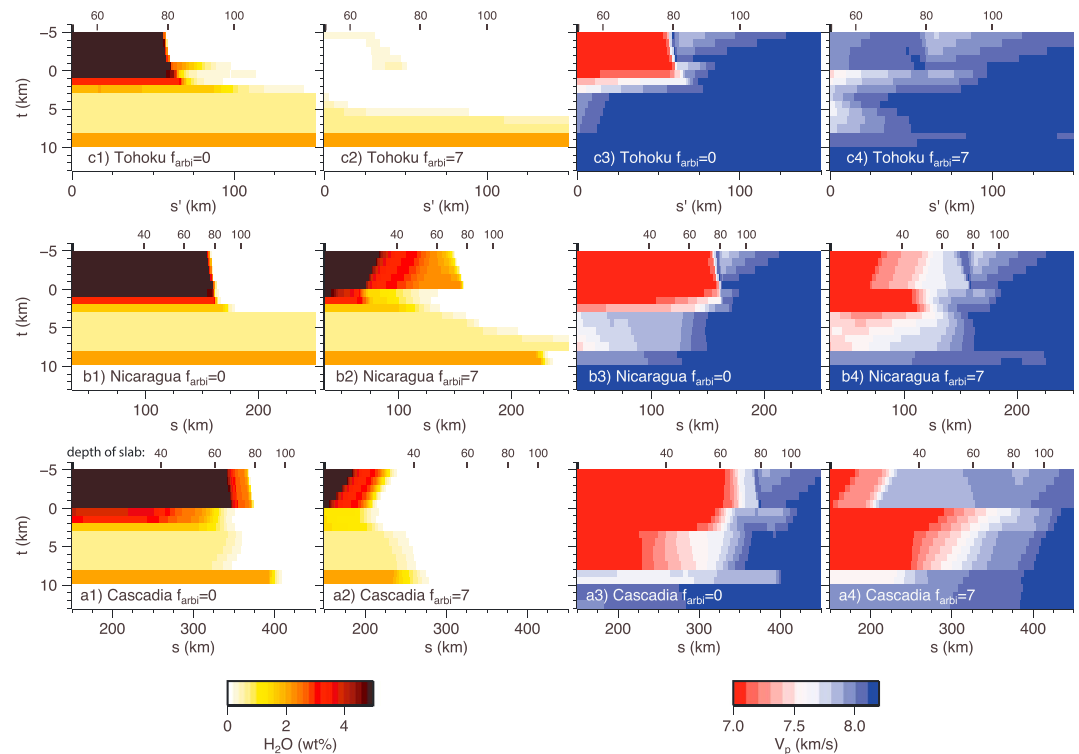
Figure 12. H_2O content and P wave speeds for the oceanic crust and surrounding mantle predicted for no arbitrary heating ($f_{arbi} = 0$) and high arbitrary heating ($f_{arbi} = 7$) and a warm, intermediate, and cold subduction zone: the Cascadia CAFE profile of Abers et al. (2013), the vK11m model for Nicaragua, and the T18 model of van Keken et al. (2012) for Tohoku. The horizontal coordinate s is distance down slab; (a and b) The origin is at the trench, and (c) it is in the slab at 55 km depth. The vertical axis is distance perpendicular to slab surface; the slab surface is at $t = 0$ km, and the oceanic Moho is at $t = 7$ km. Depth is shown at the top of each frame.

efficient dehydration of the crust below the coupling point, with a 10% reduction in the estimate of water recycled to the Earth's deep interior.

4. Discussion

When comparing the maximum PT conditions recorded by exhumed mafic subduction zone rocks to the present suite of models, it is important to recognize that the former are governed by processes that are not captured by the latter. Rocks that are exhumed are unusual for the simple reason that they escape complete subduction. Exhumation requires that a rock stalls at depth and then moves upward. At a minimum this requires buoyancy and mobility. Oceanic lithosphere is mostly buoyant when warm and before dehydration and densification begin (Hacker, 1996). Rocks within warm lithosphere are favored for exhumation. Exhumation is also more likely when subduction ceases, and downward motion and tractions no longer pull the rocks downward (e.g., Petersen & Buck, 2015).

The subduction zone thermal models presented here predict only the quasi steady state thermal structure of the OC and mantle as it is being subducted. They do not take into account exhumation or processes that have been suggested to aid exhumation—such as a change in convergence parameters (e.g., Agard et al., 2006) or subduction of thicker than normal crust (Cloos, 1993).

Models that approach the PT paths for burial and exhumation of blueschists during ongoing subduction (e.g., Burg & Gerya, 2005; Gerya et al., 2002) show, quite logically, that the forearc mantle becomes quite warm during exhumation, something quite different from the forearc structure of modern subduction zones. While short-lived exhumation periods in a *subduction channel* (e.g., Cloos, 1982) cannot be excluded, it is unlikely that exhumation is a long-lived or steady state feature of subduction zones.

Penniston-Dorland et al. (2015) argued that exhumation does not occur preferentially for young or slow subduction zones by comparing their PT estimates of specific regions to the inferred paleosubduction speeds and
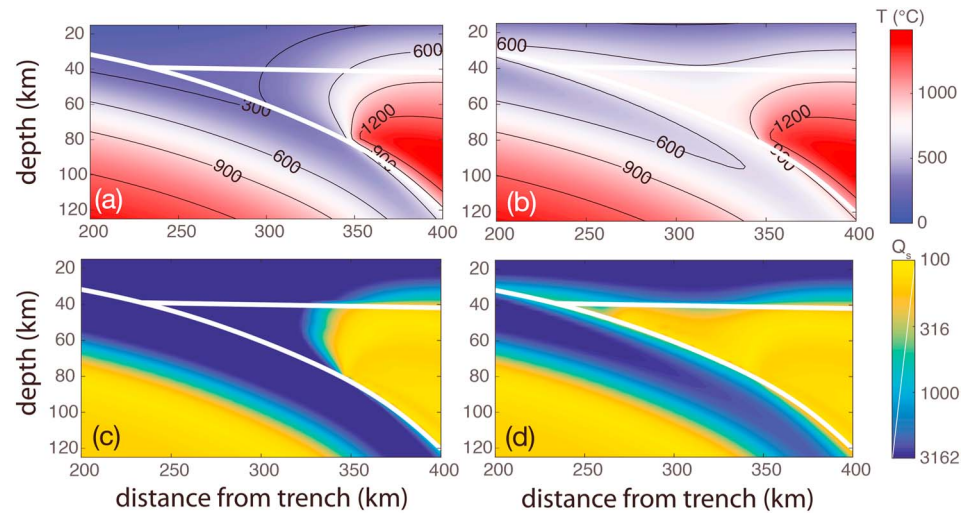
Figure 13. Effect of arbitrary shear heating on shear wave attenuation ($1/Q_s$). These attenuation predictions are based on the calibrations of Jackson and Faul (2010) modified to include the effects of H_2O as defects in olivine and of variable grain size, following Abers et al. (2014). These calculations use strain rates for the mantle wedge that are taken from the dynamical models and are set to arbitrarily low values elsewhere (10^{-19} s^{-1}). The resulting grain size distribution resembles those from the more complete calculation of Wada et al. (2011), exhibiting centimeter-scale grains in the hot wedge and smaller grain size in the high-stress cold parts of the wedge; details matter little because attenuation in cold regions is very small. (a) Temperature model for Alaska with $f_{arbi} = 0$ along the plate interface. (b) Same as (a) but for $f_{arbi} = 7$. (c) Q_s predicted for $f_{arbi} = 0$ at 1 Hz as typical for local body wave studies. (d) Q_s for $f_{arbi} = 7$.

plate ages from Agard et al. (2009). Their Figure 10 indeed shows that there is no clear correlation between paleospeeds or paleoages on the one hand and the maximum PT conditions recorded in rocks exhumed in these regions on the other. This lack of correlation is unexpected: Fast subduction and old plates must lead to colder conditions, just as slow subduction and young plates must lead to hotter conditions. The implication is that either the paleospeed and paleoplate age data are not sufficiently accurate or that the exhumed subduction zone rocks cannot be linked confidently to the reported paleoage and paleoplate speeds.

4.1. Conditions That Lead to Warmer-Than-Average Subduction Zone Temperatures

Our quasi steady state thermal models with moderate shear heating (Figures 4 and 5) satisfy a significant number of independent geophysical and geochemical constraints. Our models with high arbitrary heating that produce average PT conditions similar to that of the rock record do not. We therefore conclude that the exhumed rocks represent somewhat (up to a few 100 °C) warmer conditions than is typical of present-day mature subduction zones.

There are many occasions where these warmer conditions are a natural part of subduction zone evolution and do not require arbitrary heat sources: subduction of young oceanic lithosphere (including the subduction of small back-arc basins), the initiation of subduction, the initial evolution of the forearc mantle for young subduction systems, and the termination of subduction by slab breakoff or subduction of an mid-oceanic ridge. Three-dimensional flow effects (e.g., Bengtson & van Keken, 2012; Morishige & van Keken, 2014; Plunder et al., 2018; Wada et al., 2015) may also increase the temperature at the top of the slab, although this should not affect the forearc OC structure significantly once the cold forearc mantle has been established.

Figure 5b shows that models of subducting young oceanic lithosphere predicts average OC conditions similar to the average rock record. This has dynamic significance because newly formed oceanic lithosphere is compositionally buoyant with respect to the underlying mantle due to the low density of the crust and lower density of the harzburgite portion of the lithosphere that overlies the undepleted peridotite. This compositional buoyancy is offset by thermal contraction upon cooling for tens of millions of years after formation. Prior to that, the thermal buoyancy of the warm oceanic lithosphere can aid the exhumation of the OC. Such warm buoyant conditions can also occur during the subduction of small back-arc basins (for a review see Faccena et al., 2014).
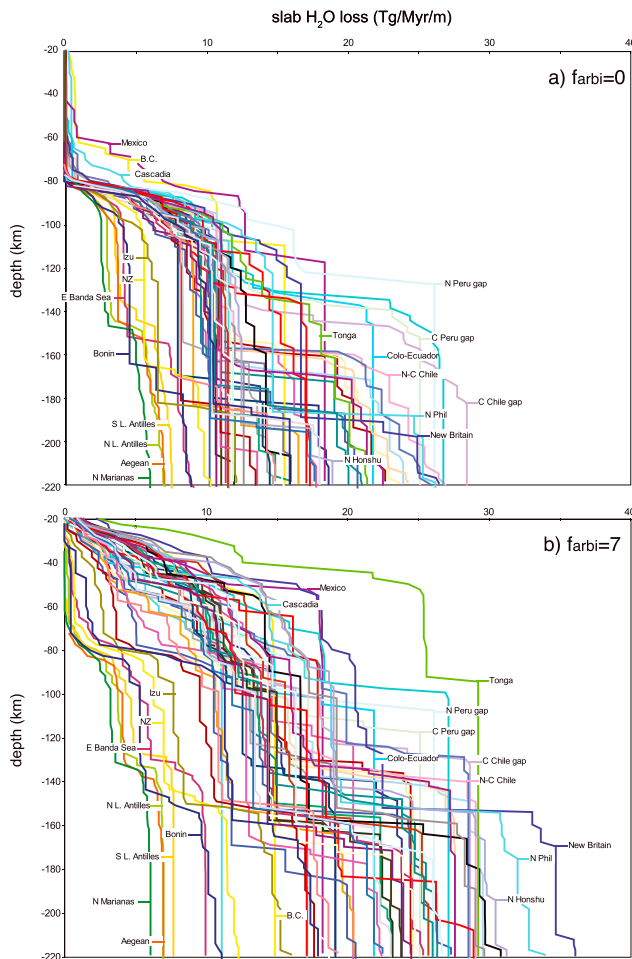
Figure 14. Cumulative water loss predicted by the vK11m models (as in Figure 6 of van Keken et al., 2011) with $f_{arbi} = 0$ and 7 (high arbitrary heating to match the rock record).

Literature estimates for the time it takes for the oceanic lithosphere to become negatively buoyant with respect to the underlying asthenosphere range from 10 to 30 Myr (Cloos, 1993; Oxburgh & Parmentier, 1977), where the higher estimate appropriately takes into account the density increase with depth in the shallow upper mantle. This age estimate varies as a function of crustal thickness (thicker crust will require longer cooling), metamorphic phase changes (blueschist and eclogite densify the crust requiring a shorter cooling period), serpentinization of the slab mantle (leading again to longer estimates for cooling), or secular variations in the temperature of the upper mantle, with warmer conditions in the past leading to the formation of thicker and more buoyant crust (van Avendonk et al., 2017; Vlaar et al., 1993).

Exhumation of mafic rocks can occur for a significant number of cases in the early stages of a subduction zone (Agard et al., 2009). During the initiation of subduction, the slab encounters a warm mantle leading to significantly warmer conditions than predicted in the vK11m and WW09m models. In addition, the evolution from subduction initiation to this steady state allows for a significant period of warmer conditions because the cooling of the forearc takes place on time scales of O(10 Myr) as discussed in section 1 (see also Maresch & Gerya, 2010). Figure 15 shows the thermal evolution of the uppermost OC in a warm, intermediate, and cold model from vK11m without shear heating. The rate of cooling depends on the slab speed and geometry, but we find that at least in the first few million years of a subduction zone the temperature in the OC falls within the PT range of the rock record for most subduction zones. We note that resetting of the forearc thermal structure can also occur after slab breakoff (Davies & von Blanckenburg, 1995; Faccena et al., 2014; Freeburn et al., 2017) and trench jumps after terrane or microcontinent accretion in regions that are otherwise characterized by long-lived subduction.

Exhumation of blueschist and eclogite has also been suggested to occur preferentially upon subduction termination (Agard et al., 2009) caused by continent-continent collision or by the mid-ocean ridge subduction. Neither is modeled in WW09m or vK11m, and any rocks that might have been caught up in such conditions should be excluded from comparison to the thermal models. Mid-ocean ridge subduction logically leads to significantly higher temperatures due to the subduction of increasingly younger oceanic lithosphere.

We note that the plate age distribution has not been constant over geologic time. For example, interpretations of a recent reconstruction of the distribution of the age of the oceanic since 200 Ma (Seton et al., 2012) show that at 100 Ma the oceans were dominated by lithosphere with an age of less than 50 Myr (see Figure 3 in Coltice et al., 2013). Subduction of such young OC is compatible with the rock record and would largely reconcile the rock record and our models without the need for large arbitrary heating along the plate interface.

4.2. Dynamical Support for Exhumation Under Warmer-Than-Average Conditions

Many metamorphic PT plots in the literature and textbooks provide a region that is labeled the *forbidden zone* (Liou et al., 2000). This generally is the region of geothermal gradients <5 °C/km that is approximately represented by the cooler of the 2σ lines in Figure 2. While there are no records of exhumed rocks that have robust PT conditions that fall within this zone (Hacker, 2006), it is reasonable to ask whether rocks are truly forbidden from entering this zone or whether rocks that enter this zone are never exhumed.

Subduction occurs because of the descent of cold lithosphere. The cooling of the lithosphere creates both negative buoyancy and stiffness. The descent of the lithosphere into the deep mantle is a consequence of such negative buoyancy and stiffness. The challenge is to explain why any metamorphosed OC survives subduction and resurfaces, rather than to explain why cold crust is irretrievably lost.
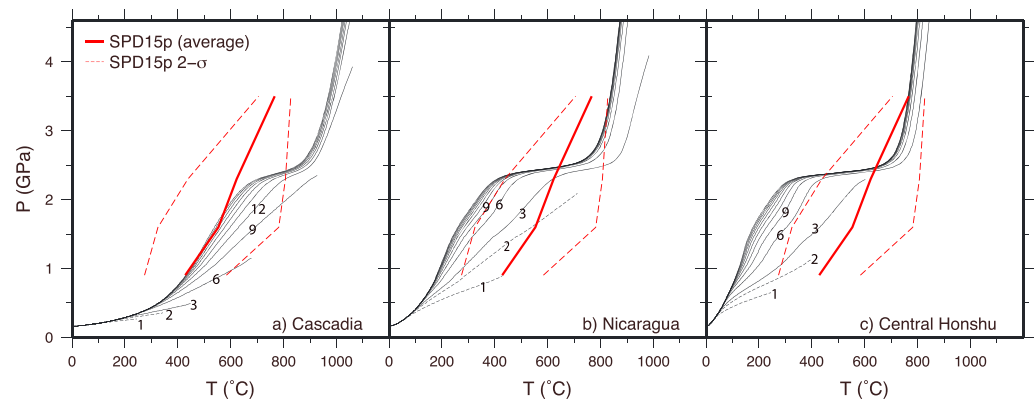
Figure 15. Temporal evolution of the temperature in the top of the OC for the (a) warm Cascadia, (b) intermediate Nicaragua, and (c) cold Tohoku models of vK11m without shear heating ($f_{arbi} = 0$). The thin dashed lines are for 1 and 2 Myr after subduction initiation. The solid lines are for 3 to 30 Myr at 3 Myr intervals. The ages for curves represented by the younger ages are indicated by the numbers. Red lines approximate the spread of pressure-temperature conditions in the rock record as in Figure 2b.

Our model predictions for the thermal structure of subducted old oceanic lithosphere show that the crust and underlying mantle remain cold to significant depths and with that retain their negative buoyancy and stiffness. Any rock from the OC needs buoyancy and mobility to overcome the coupling to the sinking slab. Higher temperatures by themselves provide both increased buoyancy due to thermal expansion and increased mobility as rock deformation is thermally activated. In addition, the higher temperatures will lead to enhanced fluid productivity due to the more efficient dehydration of the OC (Hacker, 2008; van Keken et al., 2011), which in turn leads to more efficient serpentinization and chloritization of the hanging wall and greater buoyancy and mobility (e.g., Gerya & Meilik, 2011). The greater fluid production below the forearc during warmer-than-normal conditions would logically enhance mechanical decoupling and increase the likelihood of the formation of a Cloos-style subduction zone channel (Gerya et al., 2002).

In summary, subduction environments vary in time and space. In their initial stages, most subduction zones are warm enough for the production of fluids and can likely provide sufficient buoyancy and mobility for exhumation to occur. As the forearc mantle and the slab cool, the ability to produce fluids below the forearc is lost, the slab stiffens, and the OC is lost by recycling to the deeper mantle, except perhaps for regions where young oceanic lithosphere is subducted.

5. Conclusions and Outlook

The record of exhumed subduction zone blueschists and eclogites shows average maximum PT conditions that are 200–300 °C higher at pressures of 1–2.5 GPa than the average predicted by subduction zone models. We have shown that geophysically constrained levels of shear heating along the subduction interface explains less than 50 °C of this difference. If we add much higher, and in our view unrealistically high, arbitrary heating along the subduction interface, we can reproduce in our models the average and spread of rock record, but the resulting models are in conflict with many independent geophysical and geochemical observations. We conclude that the exhumed rocks on average record higher PT conditions than the average of the PT conditions in the OC in the forearc of modern-day subduction zones. The rock record agrees well with the long-term thermal structure of young oceanic lithosphere and during the initial stages of subduction. We infer that rocks are preferentially exhumed under conditions that are on average warmer than that in present-day mature subduction zones. This inference is supported by the rare and punctuated nature of exhumation, as well as by dynamical arguments, because warmer conditions and associated fluid productivity provide buoyancy and greater mobility through thermally activated and fluid-assisted deformation.

Our suggestion that rocks are exhumed from subduction environments that are on average warmer than the present-day subduction system overlaps significantly with the conclusions from Agard et al. (2009) with one important exception. Our current suggestion does not explain the exhumation of HP/UHP rocks from subduction zones that are inferred to be mature with older oceanic lithosphere entering the trench. Examples include those from the Zagros (Agard et al., 2007; where changes in subduction forcing functions may have led to

exhumation) or for the Zermatt-Saas ophiolite, which suggests subduction of OC that formed around 160 Ma (Rubatto et al., 1998) at ~45 Ma (which even at low convergence rates should not lead to a hot subduction environment).

We note that we have taken the rock record *as is* from updates on published data sets to try to isolate maximum PT conditions in the rock record that were obtained during the prograde path. It will be important to further assess whether the maximum PT conditions truly reflect the maximum conditions during burial or that they were rather locked in during exhumation rather than burial. Literature data may also need to be corrected for reaction overstepping (Spear et al., 2014). Within this context it is also important to determine whether any of the inferred OC data may still be related to continental subduction and should therefore not be compared to the present set of thermal models. We note that the Lago di Cignana UHP coesite-eclogite facies rocks, which seem to clearly represent the uppermost OC and sediments of a subducted slab (e.g., Angiboust et al., 2009), show peak PT conditions of 600 °C at 3 GPa (Groppo et al., 2009), which falls well within the range predicted by the thermal models.

Improvements on the present study and previous global comparisons between the rock record and thermal models (Brown & Johnson, 2018; Penniston-Dorland et al., 2015) should include detailed regional comparisons that take into account the subduction history, subduction and exhumation PT(t) paths, exhumation mechanisms, and critical assessment of the available petrological, geological, and geophysical constraints.

Appendix A: Finite Element Modeling of Subduction Zone Thermal Structure

We provide two independent suites of models of subduction zone thermal structure that are based on high-resolution finite element models. The vK11m models are based on the Sepran finite element method for heat and fluid flow problems (Cuvelier et al., 1986) as described in van Keken et al. (2002) and Kneller et al. (2007). The WW09m models are based on the PGCtherm code developed by Dr. Jiangheng He at the Pacific Geoscience Centre of the Geological Survey of Canada as described in Currie et al. (2004) and Wada et al. (2008). Both finite element methods have been extensively tested for their use in predicting the thermal structure of subduction zones and show excellent agreement in a benchmark that was specifically developed for this purpose (van Keken et al., 2008).

The assumed model parameters for convergence speed, age of the oceanic lithosphere at the trench, slab dip below the arc, and thermal parameters for vK11m and WW09m are provided in Table A1. We list the models from WW09m in line with the most closely corresponding model of vK11m. The numbers in WW09m indicate their original ordering, which was based on increasing thermal parameter. The model parameters in vK11m are nearly identical to the assumptions in Syracuse et al. 2010. Minor changes include rounding the older slab ages to the nearest 5 Ma. We note that we also corrected a minor error in the Ryukyu model of Syracuse et al. (2010) and van Keken et al. (2011) where we used in the models an age of 53 Ma instead of the 27 Ma listed in the tables.

The vK11m models solve at each time step the Stokes equations (1) and (2) with updated viscosity using linear Taylor-Hood elements in the mantle wedge for discretization. The heat equation (5) is spatially discretized on linear triangles with a streamline upwind Petrov-Galerkin method. The resulting system of ordinary differential equations is propagated in time by an implicit Euler method using half the Courant-Friedrichs-Levy criterion for time step. The time step therefore depends on grid resolution and convergence speed and ranges between 0.01 and 0.13 Myr for the models presented here. The initial condition for the subducting slab is the thermal structure at the trench. For the overriding plate we assume either a young oceanic lithosphere (for regions with ocean-ocean convergence) or an appropriate continental geotherm. The thermal structure presented in this paper is after an evolution of 60 Myr for all subduction zones, which guarantees that the oceanic crustal thermal structure is in steady state. The matrix-vector systems that result from the spatial and temporal discretization are solved with the biCGStab iterative method.

For the WW09m models we assume that heat equation is steady state. The resulting system of nonlinearly coupled steady state equations (1), (2), and (5), assuming that $\partial T / \partial t = 0$, is solved by Picard iteration until the L-∞ norms between successive temperature and velocity solutions are less than 10^{-6}, which is generally reached within 200 iterations. The Stokes equation is solved with a penalty function method on nine-node isoparametric elements for velocity with compatible four-node elements for pressure. The heat equation is solved with a Galerkin least squares method. The resulting matrix-vector systems are solved by LU decomposition.

Table A1
Comparison of Model Input Parameters Between vK11m and WW09m

	vK11m						WW09m				
	V	age	Δ	$\phi/100$	$\phi'/100$		V	age	Δ	$\phi/100$	$\phi'/100$
Name	(mm/year)	(Ma)	(°)	(km)	(km)	Name	(mm/year)	(Ma)	(°)	(km)	(km)
Alaska Peninsula	59	52	45	22	31						
Alaska	49	47	42	15	23	8-Alaska	47	46	38	13	22
British Columbia	40	10	22	2	4						
Cascadia	30	10	20	1	3	1-Cascadia	43	8	40	2	3
Mexico	47	10	60	4	5	2-MexicoN	55	13	36	4	7
Guat/ElSal	67	17	57	10	12						
Nicaragua	71	27	62	17	19						
Costa Rica	75	27	59	17	20	10-CostaRica	80	24	63	17	19
Colombia-Ecuador	60	15	28	4	9	4-Colombia	46	16	38	5	7
N Peru gap	70	29	10	4	20						
C Peru gap	67	34	13	5	23						
Peru	65	42	31	14	27						
N Chile	79	46	29	18	36						
NC Chile	77	43	24	13	33	9-NChile	78	48	21	13	37
C Chile Gap	74	38	14	7	28						
C. Chile	72	32	28	11	23						
SC Chile	75	24	30	9	18						
S Chile	75	10	34	4	8	5-SChile	71	25	29	9	18
N Antilles	18	85	50	11	15						
S Antilles	18	85	42	10	15						
Scotia	61	59	65	32	36						
Aegean	15	200	31	15	30						
N Sumatra	42	48	49	15	20						
C Sumatra	40	55	46	16	22	7-Sumatra	40	50	34	11	20
S Sumatra	49	70	50	26	34						
Sunda Strait	61	85	49	39	52						
Java	68	110	46	53	75						
Bali Lombok	70	135	46	68	94						
W Banda Sea	74	100	54	60	74						
E Banda Sea	25	100	48	19	25						
New Britain	100	25	68	23	25						
Solomon	94	31	70	27	29						
N Vanuatu	52	44	71	22	23						
S Vanuatu	113	50	67	52	56						
Tonga	166	110	52	144	182						
Kermadec	65	105	56	56	68	14-Kermadec	57	100	56	47	57
New Zealand	30	100	52	24	30	12-Hikurangi	29	100	52	23	29
S Philippines	69	60	64	37	41						
N Philippines	88	32	57	24	28						
S Marianas	50	150	57	63	75	13-Mariana	30	140	61	37	42
N Marianas	15	150	62	20	23						
Bonin	32	145	63	41	46						
Izu	46	135	46	44	62	16-Izu	51	140	47	52	71
Kyushu	72	27	54	16	19	6-Kyushu	47	27	56	11	13

Table A1 (continued)

	vK11m					WW09m				
	V	age	Δ	ϕ/100	ϕ'/100		V	age	Δ	ϕ/100	ϕ'/100
Name	(mm/year)	(Ma)	(°)	(km)	(km)	Name	(mm/year)	(Ma)	(°)	(km)	(km)
Ryukyu	70	43	44	21	30						
Nankai	43	20	31	4	9	2-Nankai	44	15	36	4	7
C Honshu	83	130	34	60	108						
N Honshu	82	130	29	51	106	17-NEJapan	83	130	29	52	108
Hokkaido	75	115	42	57	86						
S Kurile	77	110	46	62	85						
N Kurile	78	105	50	63	82						
Kamchatka	75	95	51	55	71	15-Kamchatka	76	100	39	48	76
W Aleutians	50	56	56	23	28						
C Aleutians	63	56	54	29	35	11-Aleutians	54	55	50	23	30
E Aleutians	64	55	46	25	36						
Calabria	45	190	43	58	86						
average	62	70	46	29	41	average	55	61	43	22	33
median	66	55	47	22	29	median	51	48	39	13	22

Note. V is convergence speed, Δ is slab dip below the arc, ϕ is the thermal parameter (speed times age times sine of the slab dip), and ϕ' is modified thermal parameter (just speed times age). The global average of the WW09m models is warmer than same of vK11 in part because of the younger average age and lower convergence speed.

The boundary condition of the incoming plate is generally based on the plate cooling model GDH1 (Stein & Stein, 1992), which is based on a mantle potential temperature of 1421.5 °C in the vK11m models. The WW09m models with substantial (>500 m) sediment cover at the trench the temperature boundary condition incorporates the thermal effect of sedimentation on the geotherm of the cooling plate (as in Wada & Wang, 2009). With this approach the temperature at the top of the volcanics at the trench is slightly higher (up to ~50°C) compared to models that treat the sediment column as part of the cooling oceanic material (as is assumed in all models of vK11m). In WW09m we assume that the sediments do not subduct and subducting interface is defined by the top of the OC. In vK11m we assume that the sediments subduct, compact, and erode by a linear thinning with depth down to 15 km to a prescribed final sediment thickness that remains part of the subducting plate. The plate interface is here defined by the top of the sediments.

The WW09m models differ from those published in Wada and Wang 2009 by also using 1421.5 °C for potential temperature in the boundary condition used for the backarc. In both WW09m and vK11m we ignore any viscous dissipation in the mantle wedge.

Both models use a non-Newtonian viscosity for the mantle wedge, which is based on the creep laws for olivine from (Karato & Wu, 1993) that has the general form

$$\eta(T, \underline{\underline{\dot{\epsilon}}}) = A \exp\left(-\frac{E}{nRT}\right) II^{\left(\frac{1-n}{n}\right)}, \tag{A1}$$

where n is the stress exponent, E is activation energy, R is the gas constant, II is the second invariant of the strain rate tensor, and A is a prefactor. Since we ignore thermal buoyancy and viscous dissipation in the mantle wedge, the value of A does not affect the wedge flow pattern or speed, but we scale the viscosity (A1) when solving equations (1) and (2) so that the average viscosity is near unity for numerical stability. The WW09m models use $n = 3$ and $E = 435$ kJ/mol representing deformation of olivine under hydrated conditions. The vK11m models assume dislocation creep in olivine under dry conditions with $n = 3.5$ and $E = 540$ kJ/mol.

The two set of models have a significantly different approach to model the subduction interface down to the slab-wedge coupling point (which is at 75 km depth in WW09m and at 80 km depth in vK11m). For vK11m we model the interface between the slab and the overriding crust and mantle as a slipping fault, where the velocity is fully decoupled to 40 km depth. Between 40 and 80 km depth we drive wedge convection by prescribing a kinematic boundary condition that has 5% of the slab speed; the kinematic boundary assumes full slab speed below 80 km depth. For models that include heating at the top of the slab we assuming a delta

pulse of heating at the interface (van Keken et al., 2002) that has an integrated magnitude of $f_{arbi}Q_{stylized}$ (see equations (6) and (7)). WW09m assume a thin (100 m) layer along the top of the slab that has low constant viscosity causing efficient decoupling. In the models that assume shear heating the frictional heating Q_f is prescribed down to the downdip limit of the seismogenic zone (of variable depth). Below the seismogenic zone down to the slab-wedge coupling point WW09m uses a viscous dissipation term Q_d based on a quartz diorite rheology which follows (A1) with $n = 2.4$ and $E = 212$ kJ/mol (Carter & Tsenn, 1987). The prefactor A is scaled such that the magnitude of viscous dissipation matches the frictional heating at the downdip limit of the seismogenic zone, and there is a gradual transition between these two modes of shear heating (see Figure 6).

We assume that convection occurs in an incompressible Boussinesq medium. The compressibility of Earth's mantle causes a modest adiabatic temperature increase (assumed to be 0.3 °C/km). In vK11m we add this gradient a posteriori to the resulting temperature field. In WW09m we add this temperature gradient explicitly to the boundary conditions.

The overriding crust in continental subduction zones is modeled with similar internal heating as described in van Keken et al. (2002) and Wada and Wang (2009). The models employ the same assumptions for density, thermal conductivity, and specific heat (Wada & Wang, 2009).

Both models use variable resolution with that refine significantly in the thermal boundary layers and the corner of the mantle wedge (for example, vK11m generally uses 8 km size elements in the deep slab mantle and 1 km elements in the top of the slab and overriding plate). The total number of linear elements depends on the width of the model and varies between 34k and 120k in vK11m. The subduction interface is modeled as a fault, which is accurately represented by the discontinuous velocity across the interface by the finite element method.

WW09m uses a geometrical grid refinement (Currie et al., 2004; Wada & Wang, 2009) where elements range from 10 km far from the boundary layers to 1 m in the thin low viscosity channel that defines the subduction interface. A typical mesh has on the order of 10k quadratic elements.

The two modeling approaches compare rather well in the subduction zone benchmark of van Keken et al. (2008) and report, at the highest resolution used at the time, the requested spot temperatures to within 0.6 °C for the most challenging benchmark case 2b with temperature-dependent and strain rate-dependent rheology based on the rheology of dry olivine. The spatial resolution of the both sets of models presented here is sufficient to resolve the thermal structure in the subducting crust to within a few degrees.

Acronyms

WW09m   Suite of 17 subduction zone models modified from Wada and Wang (2009).

vK11m   Suite of 56 subduction zone models modified from van Keken et al. (2011).

SPD15p   Maximum PT conditions for rocks with clear prograde paths from Penniston-Dorland et al. (2015).

References

Abers, G. A., Fischer, K. M., Hirth, G., Wiens, D. A., Plank, T., Holtzman, B. K., et al. (2014). Reconciling mantle attenuation-temperature relationships from seismology, petrology and laboratory measurements. *Geochemistry, Geophysics, Geosystems*, 15, 3521–3542. https://doi.org/10.1002/2014GC005444

Abers, G. A., & Hacker, B. R. (2016). A MATLAB toolbox and Excel workbook for calculating the densities, seismic wave speeds, and major element composition of minerals and rocks at pressure and temperature. *Geochemistry, Geophysics, Geosystems*, 17, 616–624. https://doi.org/10.1002/2015GC006171

Abers, G. A., Nakajima, J., van Keken, P. E., Kita, S., & Hacker, B. R. (2013). Thermal-petrological controls on the location of earthquakes within subducting plates. *Earth and Planetary Science Letters*, 369–370, 178–187. https://doi.org/10.1016/j.epsl.2013.03.022

Abers, G. A., van Keken, P. E., & Hacker, B. R. (2017). The cold and relatively dry nature of mantle forearcs in subduction zones. *Nature Geoscience*, 10, 333–337. https://doi.org/10.1038/ngeo2922

Abers, G. A., van Keken, P. E., Kneller, E. A., Ferris, A., & Stachnik, J. C. (2006). The thermal structure of subduction zones constrained by seismic imaging: Implications for slab dehydration and wedge flow. *Earth and Planetary Science Letters*, 241, 387–397. https://doi.org/10.1016/j.epsl.2005.11.055

Agard, P., Jolivet, L., Vrielynck, B., Burov, E., & Monié, P. (2007). Plate acceleration: The obduction trigger? *Earth and Planetary Science Letters*, 258, 428–441. https://doi.org/10.1016/j.epsl.2007.04.002

Agard, P., Monié, P., Gerber, W., Omrani, J., Molinaro, M., Meyer, B., et al. (2006). Transient, synobduction exhumation of Zagros blueschists inferred from P–T, deformation, time, and kinematic constraints: Implications for Neotethyan wedge dynamics. *Journal of Geophysical Research*, 111, B11401. https://doi.org/10.1029/2005JB004103

Agard, P., Yamato, P., Jolivet, L., & Burov, E. (2009). Exhumation of oceanic blueschists and eclogites in subduction zones: Timing and mechanisms. *Earth-Science Reviews*, 92, 53–79. https://doi.org/10.1016/j.earscirev.2008.11.002

Angiboust, S., Agard, P., Jolivet, L., & Beyssac, O. (2009). The Zermatt-Saas ophiolite: The largest (60-km wide) and deepest (c. 70–80 km) continuous slice of oceanic lithosphere detached from a subduction zone? *Terra Nova*, *21*, 171–180. https://doi.org/10.1111/j.1365-3121.2009.00870.x

Arredondo, K. M., & Billen, M. I. (2017). Coupled effects of phase transitions and rheology in 2-D dynamical models of subduction. *Journal of Geophysical Research: Solid Earth*, *122*, 5813–5830. https://doi.org/10.1002/2017JB014374

Asano, Y., Saito, T., Ito, Y., Shiomi, K., Hirose, H., Matsumoto, T., et al. (2011). Spatial distribution and focal mechanisms of the aftershocks of the 2011 off the Pacific coast of Tohoku Earthquake. *Earth, Planets and Space*, *63*, 669–673. https://doi.org/10.5047/eps.2011.06.016

Bebout, G. E., & Penniston-Dorland, S. C. (2016). Fluid and mass transfer at subduction interfaces—The field metamorphic record. *Lithos*, *240-243*, 228–258. https://doi.org/10.1016/j.lithos.2015.10.007

Bengtson, A. K., & van Keken, P. E. (2012). Three-dimensional thermal structure of subduction zones: Effects of obliquity and curvature. *Solid Earth*, *3*, 365–373. https://doi.org/10.5194/se-3-365-2012

Bodri, L., & Bodri, B. (1978). Numerical investigation of tectonic flow in island-arc areas. *Tectonophysics*, *50*, 163–175. https://doi.org/10.1016/0040-1951(78)90133-6

Bose, K., & Ganguly, J. (1995). Experimental and theoretical studies of the stabilities of talc, antigorite and phase A at high pressures with applications to subduction processes. *Earth and Planetary Science Letters*, *136*, 109–121. https://doi.org/10.1016/0012-821X(95)00188-I

Bostock, M. G., Hyndman, R. D., Rondenay, S., & Peacock, S. M. (2002). An inverted continental Moho and serpentinization of the forearc mantle. *Nature*, *417*, 536–538. https://doi.org/10.1038/17536a

Brown, M., & Johnson, T. (2018). Secular change in metamorphism and the onset of global plate tectonics. *American Mineralogist*, *103*, 181–196. https://doi.org/10.2138/am-2018-6166

Burg, J.-P., & Gerya, T. V. (2005). The role of viscous heating in Barrovian metamorphism of collisional orogens: Thermomechanical models and application to the Lepontine Dome in the Central Alps. *Journal of Metamorphic Geology*, *23*, 75–95. https://doi.org/10.1111/j.1525-1314.2005.00563.x

Carter, N. L., & Tsenn, M. C. (1987). Flow properties of continental lithosphere. *Tectonophysics*, *136*, 27–63. https://doi.org/10.1016/0040-1951(87)90333-7

Chemia, Z., Dolejš, D., & Steinle-Neumann, G. (2015). Thermal effects of variable material properties and metamorphic reactions in a three-component subducting slab. *Journal of Geophysical Research: Solid Earth*, *120*, 6823–6845. https://doi.org/10.1002/2015JB012080

Christensen, U. R., & Yuen, D. A. (1985). Layered convection induced by phase transitions. *Journal of Geophysical Research*, *90*, 10,291–10,300. https://doi.org/10.1029/JB090iB12p10291

Čížková, H., & Bina, C. (2013). Effects of mantle and subduction-interface rheologies on slab stagnation and trench rollback. *Earth and Planetary Science Letters*, *379*, 95–103. https://doi.org/10.1016/j.epsl.2013.08.011

Cloos, M. (1982). Flow melanges: Numerical modeling and geologic constraints on their origin in the Franciscan subduction complex, California. *Geological Society of America Bulletin*, *93*, 330–345. https://doi.org/10.1130/0016-7606(1982)93<330:FMNMAG>2.0.CO;2

Cloos, M. (1993). Lithospheric buoyancy and collisional orogenesis: Subduction of oceanic plateaus, continental margins, island arcs, spreading ridges, and seamounts. *Geological Society of America Bulletin*, *105*, 715–737. https://doi.org/10.1130/0016-7606(1993)105<0715:LBACOS>2.3.CO;2

Coltice, N., Seton, M., Rolf, T., Müller, R. D., & Tackley, P. J. (2013). Convergence of tectonic reconstructions and mantle convection models for signficant fluctuations in seafloor spreading. *Earth and Planetary Science Letters*, *383*, 92–100. https://doi.org/10.1016/j.epsl.2013.09.032

Cook-Kollars, J., Bebout, G. E., Collins, N. C., Angiboust, S., & Agard, P. (2014). Subduction zone metamorphic pathway for deep carbon cycling: I. Evidence from HP/UHP metasedimentary rocks, Italian Alps. *Chemical Geology*, *386*, 31–48. https://doi.org/10.1016/j.chemgeo.2014.07.013

Cooper, L. B., Ruscitto, D. M., Plank, T., Wallace, P. J., Syracuse, E. M., & Manning, C. E. (2012). Global variations in H_2O/Ce: 1. Slab surface temperatures beneath volcanic arcs. *Geochemistry, Geophysics, Geosystems*, *13*, Q03024. https://doi.org/10.1029/2011GC003902

Currie, C. A., Wang, K., Hyndman, R. D., & He, J. (2004). The thermal effects of steady-state slab-driven mantle flow above a subducting slab: The Cascadia subduction zone and backarc. *Earth and Planetary Science Letters*, *223*, 35–48. https://doi.org/10.1016/j.epsl.2004.04.020

Cuvelier, C., Segal, A., & van Steenhoven, A. A. (1986). *Finite element methods and the Navier-Stokes equations*. Norwell, MA: Reidel.

Dalton, C. A., Langmuir, C. H., & Gale, A. (2014). Geophysical and geochemical evidence for deep temperature variations beneath mid-oceanic ridges. *Science*, *344*, 80–83. https://doi.org/10.1126/science.1249466

Davies, J. H., & von Blanckenburg, F. (1995). Slab breakoff: A model of lithosphere detachment and its test in the magmatism and deformation of collisional orogens. *Earth and Planetary Science Letters*, *129*, 85–102. https://doi.org/10.1016/0012-821X(94)00237-S

Dragovic, B., Baxter, E. F., & Caddick, M. J. (2015). Pulsed dehydration and garnet growth during subduction revealed by zoned garnet geochronology and thermodynamic modeling, Sifnos, Greece. *Earth and Planetary Science Letters*, *413*, 111–122. http://doi.org/10.1016/j.epsl.2014.12.024

Endo, S., Wallis, S. R., Tsuboi, M., Aoya, M., & Uehara, S.-i (2012). Slow subduction and buoyant exhumation of the Sanbagawa eclogite. *Lithos*, *146–147*, 183–201. https://doi.org/10.1016/j.lithos.2012.05.010

Erdman, M. E., & Lee, C.-T. (2014). Oceanic- and continental-type metamorphic terranes: Occurrence and exhumation mechanisms. *Earth Science Reviews*, *139*, 33–46. https://doi.org/10.1016/j.earscirev.2014.08.012

Ernst, W. G. (2003). High-pressure and ultrahigh-pressure metamorphic belts—Subduction, recrystallization, exhumation, and the significance for ophiolite study, *Ophiolite concept and volution of geological thought* (Vol. 373, pp. 365–384). Boulder: Geological Society of America, Special Paper.

Faccena, C., Becker, T. W., Auer, L., Billi, A., Boschi, L., Brun, J. P., et al. (2014). Mantle dynamics in the Mediterranean. *Reviews of Geophysics*, *52*, 283–332. https://doi.org/10.1002/2013RG000444

Freeburn, R., Bouilhol, P., Maunder, B., Magni, V., & van Hunen, J. (2017). Numerical models of the magmatic processes induced by slab breakoff. *Earth and Planetary Science Letters*, *478*, 203–213. https://doi.org/10.1016/j.epsl.2017.09.008

Gaetani, G. A., Grove, T. L., & Bryan, W. B. (1993). The influence of water on the petrogenesis of subduction-related igneous rocks. *Nature*, *365*, 332–334. https://doi.org/10.1038/365332a0

Gao, X., & Wang, K. (2014). Strength of stick-slip and creeping subduction megathrusts from heat flow observations. *Science*, *345*, 1038–1041. http://doi.org/10.1126/science.1255487

Gao, X., & Wang, K. (2017). Rheological separation of the megathrust seismogenic zone and episodic tremor and slip. *Nature*, *543*, 416–419. http://doi.org/10.1038/nature21389

Gerya, T. V., & Meilik, F. I. (2011). Geodynamic regimes of subduction under an active margin: Effects of rheological weakening by fluids and melts. *Journal of Metamorphic Geology*, *29*, 7–31. http://doi.org/10.1111/j.1525-1314.2010.00904.x

Gerya, T. V., Stöckhert, B., & Perchuk, A. L. (2002). Exhumation of high-pressure metamorphic rocks in a subduction channel: A numerical simulation. *Tectonics*, *21*(6), 1056. http://doi.org/10.1029/2002TC001406

Groppo, C., Beltrando, M., & Compagnoni, R. (2009). The P-T path of the ultra-high pressure Lago Di Cignana and adjoining high-pressure meta-ophiolitic units: Insights into the evolution of the subducting Tethyan slab. *Journal of Metamorphic Geology*, *27*, 207–231. https://doi.org/10.1111/j.1525-1314.2009.00814.x

Grove, T. L., Chatterjee, N., Parman, S. W., & Médard, E. (2006). The influence of H_2O on mantle wedge melting. *Earth and Planetary Science Letters*, *249*, 74–89. 2006. https://doi.org/10.1016/j.epsl.2006.06.043

Hacker, B. R. (1996). Eclogite formation and the rheology, buoyancy, seismicity, and H_2O content of the oceanic crust. In G. E. Bebout, D. Scholl, S. H. Kirby, & J. P. Platt (Eds.), *Subduction top to bottom, Geophysical Monograph Series* (Vol. 96, pp. 337–346). Washington, DC: American Geophysical Union.

Hacker, B. R. (2006). Pressures and temperatures of ultrahigh-pressure metamorphism: Implications for UHP tectonics and H_2O in subducting slabs. *International Geology Review*, *48*, 1053–1066. https://doi.org/10.2747/0020-6814.48.12.1053

Hacker, B. R. (2008). H_2O subduction beyond arcs. *Geochemistry, Geophysics, Geosystems*, *9*, Q03001. https://doi.org/10.1029/2007GC001707

Hacker, B. R., Peacock, S. M., Abers, G. M., & Holloway, S. D. (2003). Subduction factory 2. Are intermediate-depth earthquakes in subducting slabs linked to metamorphic dehydration reactions? *Journal of Geophysical Research*, *108*(B1), 2030. https://doi.org/10.1029/2001JB001129

Hansen, S. M., Schmandt, B., Levander, A., Kiser, E., Vidale, J. E., Abers, G. A., & Creager, K. C. (2016). Seismic evidence for a cold serpentinized mantle wedge beneath Mount St Helens. *Nature Communications*, *7*, 13242. https://doi.org/10.1038/ncomms13242

Hermann, J., Müntener, O., & Scambelluri, M. (2000). The importance of serpentinite mylonites for subduction and exhumation of oceanic crust. *Tectonophysics*, *327*, 225–238. https://doi.org/10.1016/S0040-1951(00)00171-2

Hermann, J., & Spandler, C. J. (2007). Sediment melts at sub-arc depths: An experimental study. *Journal of Petrology*, *49*, 717–740. 2008. https://doi.org/10.1093/petrology/egm073

Herzberg, C., Asimow, P. D., Arndt, N., Niu, Y., Lesher, C. M., Fitton, J. G., et al. (2007). Temperatures in ambient mantle and plumes: Constraints from basalts, picrites, and komatiites. *Geochemistry, Geophysics, Geosystems*, *8*, Q02006. https://doi.org/10.1029/2006GC001390

Hilairet, N., Daniel, I., & Reynard, B. (2006). Equation of state of antigorite, stability field of serpentines, and seismicity in subduction zones. *Geophysical Research Letters*, *33*, L02302. https://doi.org/10.1029/2005GL024728

Holland, G., & Ballentine, C. J. (2006). Seawater subduction controls the heavy noble gas composition of the mantle. *Nature*, *441*, 186–191. https://doi.org/10.1038/nature04761

Hyndman, R. D., & Peacock, S. M. (2003). Serpentinization of the forearc mantle. *Earth and Planetary Science Letters*, *212*, 417–432. https://doi.org/10.1016/S0012-821X(03)00263-2

Igarashi, T., Matsuzawa, T., Umino, N., & Hasegawa, A. (2001). Spatial distribution of focal mechanisms for interplate and intraplate earthquakes associated with the subducting Pacific plate beneath the northeastern Japan arc: A triple-planed deep seismic zone. *Journal of Geophysical Research*, *106*, 2177–2191. https://doi.org/10.1029/2000JB900386

Jackson, I., & Faul, U. H. (2010). Grainsize-sensitive viscoelastic relaxation in olivine: Toward a robust laboratory-based model for seismological application. *Physics of the Earth and Planetary Interiors*, *183*, 151–163. https://doi.org/10.1016/j.pepi.2010.09.005

Jarvis, G. T., & McKenzie, D. P. (1980). Convection in a compressible fluid with infinite Prandtl number. *Journal of Fluid Mechanics*, *96*, 515–583. https://doi.org/10.1017/S002211208000225X

Johnson, M. C., & Plank, T. (1999). Dehydration and melting experiments constrain the fate of subducted sediments. *Geochemistry, Geophysics, Geosystems*, *1*, 1007. https://doi.org/10.1029/1999GC000014

Karato, S., & Wu, P. (1993). Rheology of the upper mantle: A synthesis. *Science*, *260*, 771–778. https://doi.org/10.1126/science.260.5109.771

King, S. D., Lee, C., van Keken, P. E., Leng, W., Zhong, S., Tan, E., et al. (2010). A community benchmark for 2-D Cartesian compressible convection in the Earth's mantle. *Geophysical Journal International*, *180*, 73–87. https://doi.org/10.1111/j.1365-246X.2009.04413.x

Kirby, S. H., Durham, W. B., & Stern, L. A. (1991). Mantle phase changes and deep-earthquake faulting in subducting lithosphere. *Science*, *252*, 216–225. https://doi.org/10.1126/science.252.5003.216

Klemd, R., John, T., Scherer, E. E., Rondenay, S., & Gao, J. (2011). Changes in dip of subducted slabs at depth: Petrological and geochronological evidence from HP-UHP rocks (Tianshan, NW-China). *Earth and Planetary Science Letters*, *310*, 9–20. https://doi.org/10.1016/j.epsl.2011.07.022

Kneller, E. A., van Keken, P. E., Katayama, I., & Karato, S. (2007). Stress, strain, and B-type olivine fabric in the fore-arc mantle: Sensitivity tests using high resolution steady-state subduction zone models. *Journal of Geophysical Research*, *112*, B04406. https://doi.org/10.1029/2006JB004544

Lamb, S. (2006). Shear stresses on megathrusts: Implication for mountain building behind subduction zones. *Journal of Geophysical Research*, *111*, B07401. https://doi.org/10.1029/2005JB003916

Lee, C., & King, S. D. (2009). Effect of mantle compressibility on the thermal and flow structures of the subduction zones. *Geochemistry, Geophysics, Geosystems*, *10*, Q01006. https://doi.org/10.1029/2008GC002151

Lee, C.-T. A., Luffi, P., Plank, T., Dalton, H., & Leeman, W. P. (2009). Constraints on the depths and temperatures of basaltic magma generation on Earth and other terrestrial planets using new thermobarometers for mafic magmas. *Earth and Planetary Science Letters*, *279*, 20–33. https://doi.org/10.1016/j.epsl.2008.12.020

Liou, J. G., Hacker, B. R., & Zhang, R. Y. (2000). Into the forbidden zone. *Science*, *287*, 1215–1216. https://doi.org/10.1126/science.287.5456.1215

Maresch, W. V., & Gerya, T. V. (2010). Blueschists and blue amphiboles: How much subduction do they need? *International Geology Review*, *47*, 688–702. https://doi.org/10.2747/0020-6814.47.7.688

Molnar, P., Freedman, D., & Shih, J. S. F. (1979). Lengths of intermediate and deep seismic zones and temperatures in downgoing slabs of lithosphere. *Geophysical Journal International*, *56*, 41–54. https://doi.org/10.1111/j.1365-246X.1979.tb04766.x

Morishige, M., & van Keken, P. E. (2014). Along-arc variation in the 3-D thermal structure around the junction between the Japan and Kurile arcs. *Geochemistry, Geophysics, Geosystems*, *15*, 2225–2240. https://doi.org/10.1002/2014gc005394

Nakajima, J., Hada, S., Hayami, E., Uchida, N., Hasegawa, A., Yoshioka, S., et al. (2013). Seismic attenuation beneath northeastern Japan: Constraints on mantle dynamics and arc magmatism. *Journal of Geophysical Research: Solid Earth*, *118*, 5838–5855. https://doi.org/10.1002/2013JB010388

Oxburgh, E. R., & Parmentier, E. M. (1977). Compositional and density stratification in oceanic lithosphere—Causes and consequences. *Journal of the Geological Society*, *133*, 343–355. https://doi.org/10.1144/gsjgs.133.4.0343

Padrón-Navarta, J. A., Hermann, J., Garrido, C. J., López Sánchez-Vizcaíno, V., & Gómez-Pugnaire, M. T. (2010). An experimental investigation of antigorite dehydration in natural silica-enriched serpentinite. *Contributions to Mineralogy and Petrology*, *159*, 25–42. https://doi.org/10.1007/s00410-009-0414-5

Padrón-Navarta, J. A., López Sánchez-Vizcaíno, V., Hermann, J., Connolly, J. A. D., Garrido, C. J., Gómez-Pugnaire, M. T., & Marchesi, C. (2013). Tschermak's substitution in antigorite and consequences for phase relations and water liberation in high-grade serpentinites. *Lithos*, *178*, 186–196. https://doi.org/10.1016/j.lithos.2013.02.001

Parai, R., & Mukhopadhyay, S. (2012). How large is the subducted water flux? New constraints on mantle regassing rates. *Earth and Planetary Science Letters*, *317–318*, 396–406. https://doi.org/10.1016/j.epsl.2011.11.024

Peacock, S. M. (1996). Thermal and petrological structure of subduction zones. In G. E. Bebout, D. W. Scholl, S. H. Kirby, & J. P. Platt (Eds.), *Subduction: Top to bottom, Geophysical Monograph Series* (Vol. 96, pp. 119–133). Washington, DC: American Geophysical Union. https://doi.org/10.1029/GM096p0119

Peacock, S. M., Rushmer, T., & Thompson, A. B. (1994). Partial melting of subducting oceanic crust. *Earth Planetary Science Letters*, *121*, 227–244. https://doi.org/10.1016/0012-821X(94)90042-6

Peacock, S. M., & Wang, K. (1999). Seismic consequences of warm versus cool subduction metamorphism: Examples from Southwest and Northeast Japan. *Science*, *286*, 937–939. https://doi.org/10.1126/science.286.5441.937

Penniston-Dorland, S. C., Bebout, G. E., Pogge von Strandmann, P. A. E., Elliott, T., & Sorensen, S. S. (2012). Lithium and its isotopes as tracers of subduction zone fluids and metasomatic processes: Evidence from the Catalina Schist, California, USA. *Geochimica and Cosmochimica Acta*, *77*, 530–545. https://doi.org/10.1016/j.gca.2011.10.038

Penniston-Dorland, S. C., Kohn, M. J., & Manning, C. E. (2015). The global range of subduction zone thermal structures from exhumed blueschists and eclogites: Rocks are hotter than models. *Earth Planetary Science Letters*, *428*, 243–254. https://doi.org/10.1016/j.epsl.2015.07.031

Petersen, K. D., & Buck, W. R. (2015). Eduction, extension, and exhumation of ultrahigh-pressure rocks in metamorphic core complexes due to subduction initiation. *Geochemistry, Geophysics, Geosystems*, *16*, 2564–2581. https://doi.org/10.1002/2015GC005847

Plank, T., Cooper, L. B., & Manning, C. (2009). Emerging geothermometers for estimating slab surface temperatures. *Nature Geoscience*, *2*, 611–615. https://doi.org/10.1038/ngeo614

Plank, T., Kelley, K. A., Zimmer, M. M., Hauri, E. H., & Wallace, P. J. (2013). Why do mafic arc magmas contain 4 wt% water on average? *Earth Planetary Science Letters*, *364*, 168–179. https://doi.org/10.1016/j.epsl.2012.11.044

Plunder, A., Thieulot, C., & van Hinsbergen, D. J. J. (2018). The effect of obliquity on temperature in subduction zones: Insights from 3-D numerical modeling. *Solid Earth*, *9*, 759–776. https://doi.org/10.5194/se-9-759-2018

Pollack, H. N., Hurter, S. J., & Johnson, J. R. (1993). Heat flow from the Earth's interior: Analysis of the global data set. *Reviews of Geophysics*, *31*, 267–280. https://doi.org/10.1029/93RG01249

Rubatto, D., Gebauer, D., & Fanning, M. (1998). Jurassic formation and Eocene subduction of the Zermatt-Saas-Fee ophiolites: Implications for the geodynamic evolution of the Central and Western Alps. *Contributions to Mineralogy and Petrology*, *132*, 269–287. https://doi.org/10.1007/s004100050421

Rychert, C. A., Fischer, K. M., Abers, G. A., Plank, T., Syracuse, E., Protti, J. M., et al. (2008). Strong along-arc variations in attenuation in the mantle wedge beneath Costa Rica and Nicaragua. *Geochemistry, Geophysics, Geosystems*, *9*, Q10S10. https://doi.org/10.1029/2008GC002040

Sacks, I. S. (1975). Anomalous island arc asthenosphere and continental growth. *Carnegie Institution of Washington Year Book*, *74*, 256–266. https://archive.org/details/yearbookcarne74197475carn

Saita, H., Nakajima, J., Shiina, T., & Kimura, J.-I. (2015). Slab-derived fluids, fore-arc hydration, and sub-arc magmatism beneath Kyushu, Japan. *Geophysical Research Letters*, *42*, 1685–1693. https://doi.org/10.1002/2015GL063084

Scambelluri, M., Bebout, G. E., Belmonte, D., Gilio, M., Campomenosi, N., Collins, N., & Crispini, L. (2016). Carbonation of subduction-zone serpentinite (high-pressure ophicarbonate; Ligurian Western Alps) and implication for deep carbon cycling. *Earth and Planetary Science Letters*, *441*, 155–166. https://doi.org/10.1016/j.epsl.2016.02.034

Scambelluri, M., Pettke, T., & Cannaò, E. (2015). Fluid-related inclusions in Alpine high-pressure peridotite reveal trace element recycling during subduction-zone dehydration of serpentinized mantle (Cima di Gagnone, Swiss Alps). *Earth and Planetary Science Letters*, *429*, 45–59. https://doi.org/10.1016/j.epsl.2015.07.060

Schmidt, M. W., & Poli, S. (1998). Experimentally based water budgets for dehydrating slabs and consequences for arc magma generation. *Earth and Planetary Science Letters*, *163*, 361–379. https://doi.org/10.1016/S0012-821X(98)00142-3

Scholz, C. H. (1998). Earthquakes and friction laws. *Nature*, *391*, 37–42. https://doi.org/10.1038/34097

Schubert, G., Turcotte, D. L., & Olson, P. (2001). *Mantle convection in the Earth and planets*. Cambridge, UK: University Press.

Seton, M., Müller, R. D., Zahirovic, S., Gaina, C., Torsvik, T., Shephard, G., et al. (2012). Global continental and ocean basin reconstructions since 200 Ma. *Earth-Science Reviews*, *113*, 212–270. https://doi.org/10.1016/j.earscirev.2012.03.002

Shiina, T., Nakajima, J., & Matsuzawa, T. (2013). Seismic evidence for high pore pressures in the oceanic crust: Implications for fluid-related embrittlement. *Geophysical Research Letters*, *40*, 2006–2010. https://doi.org/10.1002/grl.50468

Shiina, T., Nakajima, J., Matsuzawa, T., Toyokuni, G., & Kita, S. (2017). Depth variations in seismic velocity in the subducting crust: Evidence for fluid-related embrittlement for intermediate-depth earthquakes. *Geophysical Research Letters*, *44*, 810–817. https://doi.org/10.1002/2016GL071798

Shimamoto, T., & Noda, H. (2014). A friction to flow constitutive law and its application to a 2-D modeling of earthquakes. *Journal of Geophysical Research: Solid Earth*, *119*, 8089–8106. https://doi.org/10.1002/2014JB011170

Skora, S., & Blundy, J. (2010). High-pressure hydrous phase relations of radiolarian clay and implications for the involvement of subducted sediment in arc magmatism. *Journal of Petrology*, *51*, 2211–2243. https://doi.org/10.1093/petrology/egq054

Spear, F. S., Thomas, J. B., & Hallett, B. W. (2014). Overstepping the garnet isograd: A comparison of QuiG barometry and thermodynamic modeling. *Contributions to Mineralogy and Petrology*, *168*, 1059. https://doi.org/10.1007/s00410-014-1059-6

Spinelli, G. A., & Wang, K. (2009). Links between fluid circulation, temperature, and metamorphism in subducting slabs. *Geophysical Research Letters*, *36*, L13302. https://doi.org/10.1029/2009GL038706

Stein, C. A., & Stein, S. (1992). A model for the global variation in oceanic depth and heat flow with lithospheric age. *Nature*, *359*, 123–129. https://doi.org/10.1038/359123a0

Stepanov, A. S., Rubatto, D., Hermann, J., & Korsakov, A. V. (2016). Contrasting P-T paths within the Barchi-Kol UHP terrain (Kokchetav Complex): Implications for subduction and exhumation of continental crust. *American Mineralogist*, *101*, 788–807. https://doi.org/10.2138/am-2016-5454

Syracuse, E. M., & Abers, G. A. (2006). Global compilation of variations in slab depth beneath arc volcanoes and implications. *Geochemistry, Geophysics, Geosystems*, *7*, Q05017. https://doi.org/10.1029/2005GC001045

Syracuse, E. M., van Keken, P. E., & Abers, G. A. (2010). The global range of subduction zone thermal models. *Physics of the Earth and Planetary Interiors*, *183*, 73–90. https://doi.org/10.1016/j.pepi.2010.02.004

Tanaka, A., Yamano, M., Yano, Y., & Sasada, M. (2004). Geothermal gradient and heat flow data in and around Japan (I). *Earth, Planets, Space*, *56*, 1191–1194. https://doi.org/10.1186/BF03353339

Tatsumi, Y. (1986). Formation of the volcanic front in subduction zones. *Geophysical Research Letters*, *13*, 717–720. https://doi.org/10.1029/GL013i008p00717

Tichelaar, B. W., & Ruff, L. J. (1993). Depth of seismic coupling along subduction zones. *Journal of Geophysical Research*, *98*, 2017–2037. https://doi.org/10.1029/92JB02045

Till, C. B., Grove, T. L., & Withers, A. C. (2012). The beginnings of hydrous mantle wedge melting. *Contributions to Mineralogy and Petrology*, *163*, 669–688. https://doi.org/10.1007/s00410-011-0692-6

Tsujimori, T., & Ernst, W. G. (2014). Lawsonite blueschists and lawsonite eclogites as proxies for palaeo-subduction zone processes: A review. *Journal of Metamorphic Geology*, *32*, 437–454. https://doi.org/10.1111/jmg.12057

van Avendonk, H. J. A., Davis, J. K., Harding, J. L., & Lawver, L. A. (2017). Decrease in oceanic crustal thickness since the breakup of Pangaea. *Nature Geoscience*, *10*, 58–61. https://doi.org/10.1038/NGEO2849

van Keken, P. E., Currie, C., King, S. D., Behn, M. D., Cagnioncle, A., He, J., et al. (2008). A community benchmark for subduction zone modeling. *Physics of the Earth and Planetary Interiors*, *171*, 187–197. https://doi.org/10.1016/j.pepi.2008.04.015

van Keken, P. E., Hacker, B. R., Syracuse, E. M., & Abers, G. A. (2011). Subduction factory 4: Depth-dependent flux of H_2O from subducting slabs worldwide. *Journal of Geophysical Research*, *116*, B01401. https://doi.org/10.1029/2010JB007922

van Keken, P. E., Kiefer, B., & Peacock, S. M. (2002). High-resolution models of subduction zones: Implications for mineral dehydration reactions and the transport of water to the deep mantle. *Geochemistry, Geophysics, Geosystems*, *3*(10), 1056. https://doi.org/10.1029/2001GC000256

van Keken, P. E., Kita, S., & Nakajima, J. (2012). Thermal structure and intermediate-depth seismicity in the Tohoku-Hokkaido subduction zones. *Solid Earth*, *3*, 355–364. https://doi.org/10.5194/se-3-355-2012

Vitale Brovarone, A., & Agard, P. (2013). True metamorphic isograds or tectonically sliced metamorphic sequences? New high-spatial resolution petrological data for the New Caledonia case study. *Contributions to Mineralogy and Petrology*, *166*, 451–469. https://doi.org/10.1007/s00410-013-0885-2

Vlaar, N. J., van Keken, P. E., & van den Berg, A. P. (1993). Cooling of the earth in the Archaean: Consequences of pressure-release melting in a hotter mantle. *Earth and Planetary Science Letters*, *121*, 1–18. https://doi.org/10.1016/0012-821X(94)90028-0

Wada, I., Behn, M. D., & He, J. (2011). Grain-size distribution in the mantle wedge of subduction zones. *Journal of Geophysical Research*, *116*, B10203. https://doi.org/10.1029/2011JB008294

Wada, I., He, J., Hasegawa, A., & Nakajima, J. (2015). Mantle wedge flow pattern and thermal structure in Northeast Japan: Effects of oblique subduction and 3–D geometry. *Earth and Planetary Science Letters*, *426*, 76–88. https://doi.org/10.1016/j.epsl.2015.06.021

Wada, I., & Wang, K. (2009). Common depth of slab-mantle decoupling: Reconciling diversity and uniformity of subduction zones. *Geochemistry, Geophysics, Geosystems*, *10*, Q10009. https://doi.org/10.1029/2009GC002570

Wada, I., Wang, K., He, J., & Hyndman, R. D. (2008). Weakening of the subduction interface and its effects on surface heatflow, slab dehydration, and mantle wedge serpentinization. *Journal of Geophysical Research*, *113*, B04402. https://doi.org/10.1029/2007JB005190

Wallace, P. J. (2005). Volatiles in subduction zone magmas: Concentrations and fluxes based on melt inclusion and volcanic gas data. *Journal of Volcanology and Geothermal Research*, *140*, 217–240. https://doi.org/10.1016/j.jvolgeores.2004.07.023

Wallis, S. R., Anczkiewicz, R., Endo, S., Aoya, M., Platt, J. P., Thirlwall, M., & Hirata, T. (2009). Plate movements, ductile deformation and geochronology of the Sanbagawa belt, SW Japan: tectonic significance of 89–88 Ma Lu-Hf eclogite ages. *Journal of Metamorphic Geology*, *27*, 93–105. https://doi.org/10.1111/j.1525-1314.2008.00806.x

Walowski, K. J., Wallace, P. J., Clynne, M. A., Rasmussen, D. J., & Weis, D. (2016). Slab melting and magma formation beneath the southern Cascade arc. *Earth Planetary Science Letters*, *446*, 100–112. https://doi.org/10.1016/j.epsl.2016.03.044

Walowski, K. J., Wallace, P. J., Hauri, E. H., Wada, I., & Clynne, M. A. (2015). Slab melting beneath the Cascade Arc driven by dehydration of altered oceanic peridotite. *Nature Geoscience*, *8*, 404–408. https://doi.org/10.1038/ngeo2417

Wang, K., & Bilek, S. L. (2014). Invited review paper: Fault creep caused by subduction of rough seafloor relief. *Tectonophysics*, *610*, 1–24. https://doi.org/10.1016/j.tecto.2013.11.024

Wang, K., & He, J. (1999). Mechanics of low-stress forearcs: Nankai and Cascadia. *Journal of Geophysical Research*, *104*, 15,191–15,205. https://doi.org/10.1029/1999JB900103

Wang, K., Mulder, T., Rogers, G. C., & Hyndman, R. D. (1995). Case for very low coupling stress on the Cascadia subduction fault. *Journal of Geophysical Research*, *100*, 12,907–12,918. https://doi.org/10.1029/95JB00516

Wells, R., Bukry, D., Friedman, R., Pyle, D., Duncan, R., Haeussler, P., & Wooden, J. (2014). Geologic history of Siletzia, a large igneous province in the Oregon and Washington Coast Range: Correlation to the geomagnetic polarity time scale and implications for a long-lived Yellowstone hotspot. *Geosphere*, *10*, 692–719. https://doi.org/10.1130/GES01018.1

Wilson, C. R., Spiegelman, M., van Keken, P. E., & Hacker, B. R. (2014). Fluid flow in subduction zones: The role of solid rheology and compaction pressure. *Earth and Planetary Science Letters*, *401*, 261–274. https://doi.org/10.1016/j.epsl.2014.05.052